Millimeter-Wave Wide Band Antenna Array for 5G Mobile Applications

by

Lixia Chen

A thesis submitted to the Ottawa Carleton Institute for Electrical and Computer Engineering

in partial fulfillment to the thesis requirement for the degree of

MASTER OF APPLIED SCIENCE

in

ELECTRICAL ENGINEERING

uOttawa

University of Ottawa

Ottawa, Ontario, Canada

ABSTRACT

The thesis presents a compact, miniature, and low cost antenna array designed for millimeter-wave frequencies for future 5th generation (5G) mobile applications. The proposed antenna array is a geometrically modified structure of the Franklin array, which allowed to transform a conventional narrowband array into a wideband antenna array. It is composed of five millimetre-wave circular patch radiation elements with phasing stubs.

The designed array, fabricated on the commercial Rogers RO3003 substrate with small form factor of 8x25x0.5 mm^3, covers the upcoming 5G band of 23.6-30.3 GHz, with peak gain as 10.8 dB, and high radiation efficiency over the whole operating band. In addition, with frequency sweeping, the proposed antenna array radiation pattern is directive and offers beam steering at the desired angles, acting similarly as a leaky-wave antenna.

Keywords— 5G, Franklin array, Beam steering, Millimeter wave, Phased array, Patch array.

ACKNOWLEDGEMENTS

Contents

List of Figures

List of Tables

List of Variables

AR	Axial ratio
B	Magnetic flux density,
D	Electric flux density
E	Electric field intensity
e_a	Total antenna efficiency
e_{rad}	Radiation efficiency
e_{ref}	Reflection efficiency
ε_e	Effective dielectric constant
ε_r	Dielectric constant of substrate
ϕ	Azimuth angle
Γ	Reflection coefficient
H	Magnetic field intensity
h	Height of dielectric substrate
J	Electric current density.
L	Rectangular patch length
L_e	Effective length
λ_O	Free space wavelength
μ_o	Free-space permeability (4π x 10-7 F/m)
P	Volume change density
Pin	Input power
P_o	Ohmic losses power
Pref	Reflected power
P_r	Radiated power
Q	Quality factor

Q_c	Q-fa ctor due to conductor losses
Q_d	Q-factor, due to the dielectric loss,
Q_{sp}	Q-factor due to the space wave component
Q_{sw}	Q-factor due to the surface wave component of the antenna radiation
R_a	Antenna resistance
$R_{in\,Patch\,edge}$	Edge antenna resistance
Ro	Conduction and dielectric ohmic losses
R_r	Radiation resistance
S	Feed line inset length
σ	Conductivity
$tan\,\delta$	Loss tangent of the substrate
θ	Elevation angle
U_o	Isotropic source radiation intensity
$U(\theta,\phi)$	Given direction radiation intensity
$D(\theta,\phi)$	Directivity
W	Width of the patch
X_a	Antenna reactance
Xs	Source reactance

List of Acronyms

1G	First generation.
2G	Second generation.
3G	Third generation (3G).
4G	Fourth Generation.
5G	Fifth generation.
AiP	Antenna-in-Package.
AMTS	Advanced Mobile Telephone System.
AoD	Antenna-on-Display.
BS	Base station.
CAA	Connected antenna arrays.
CDMA	Code Division Multiple Access.
DDM	Domain Decomposition Method
DRA	Dielectric resonator antenna.
DTC	Digitally tunable capacitors.
EDGE	Enhanced Data rates for GSM Evolution.
eMBB	enhanced Mobile Broadband.
FCC	Federal Communication Committee.
FDMA	Frequency Division Multiple Access.
FDTD	Finite Differences in the Time Domain.
FEM	Finite elements Mothed.
FIT	Finite Integration Technique.
GPRS	General Packet Radio Services.
HBs	High frequency bands.
IE	Integral Equations.

IMTS	Improved Mobile Telephone Service.
ITU	International Telecommunication Union (ITU).
LDPA	Log Periodic Dipole Array
LMDS	Local Multipoint Distribution Service.
LWA	Leakage Wave Antenna
LTE	Long Term Evolution.
LTE-LAA	LTE licensed assisted access.
MIMO	Multiple Input Multiple Output.
ML	Mismatch loss.
mMTC	massive Machine Type Communications.
mm-Wave	millimetre-wave.
MoM	Method of Moments.
MTS	Mobile Telephone System.
OFDMA	Orthogonal Frequency Division Multiple Access.
PTT	Push to Talk.
RF	Radio Frequency.
RL	Return loss.
SIW	Substrate Integrated Waveguide
TDMA	Time Division Multiple Access.
UE	User equipment.
UMTS	Universal Mobile Telecommunication System).
uRLLC	ultra Reliable Low Latency Communication.
VSWR	Voltage Standing Wave Ratio.

Chapter 1. Introduction

1.1 Technologies Evolution

Since the first generation of mobile network standards published in 1982, a new standard generation comes along each 10 years or so. To serve the technology demands, mobile communication has experienced remarkable evolution over recent decades: from first generation technology to current fourth generation technology, there are significant changes in the nature of hardware, user data throughput, telecommunication technology, licensed and unlicensed frequency spectrum, and latency (Figure 1) [1][2].

The so-called "First generation" or "1G" of communication systems was deployed in the 1980s and supported voice transmission only. In addition, there were significant differences between countries and areas or telecommunication service providers in terms of technologies and protocols. Different mobile technologies were introduced such as Mobile Telephone System (MTS), Advanced Mobile Telephone System (AMTS), Improved Mobile Telephone Service (IMTS), and Push to Talk (PTT)[1]. These systems mainly used analog Radio Frequency (RF) signals, with Frequency Division Multiple Access (FDMA) scheme to divide the bandwidth into specific channel frequencies that can be assigned to individual users. However, they exhibited low capacity, unreliable handoff, poor voice links, and low security.

The Second generation (2G) was introduced in the late 1980s, where the systems used digital signals for voice transmission, with either TDMA (Time Division Multiple Access) or CDMA (Code Division Multiple Access) methods. Later, the following 2.5G systems, i.e., GPRS (General Packet Radio Services), CDMA, and EDGE (Enhanced Data rates for GSM Evolution), used packet switched and circuit switched domains.

The Third generation (3G) emerged in 2000 with significant changes in terms of technology. 3G mobile system was then named as UMTS (Universal Mobile Telecommunication System) in Europe with Wideband-CDMA as standard, while CDMA emerged in the American market.

Figure 1 shows a general picture of how 5G impacts on the data rates compares with current 3G and 4G technologies,
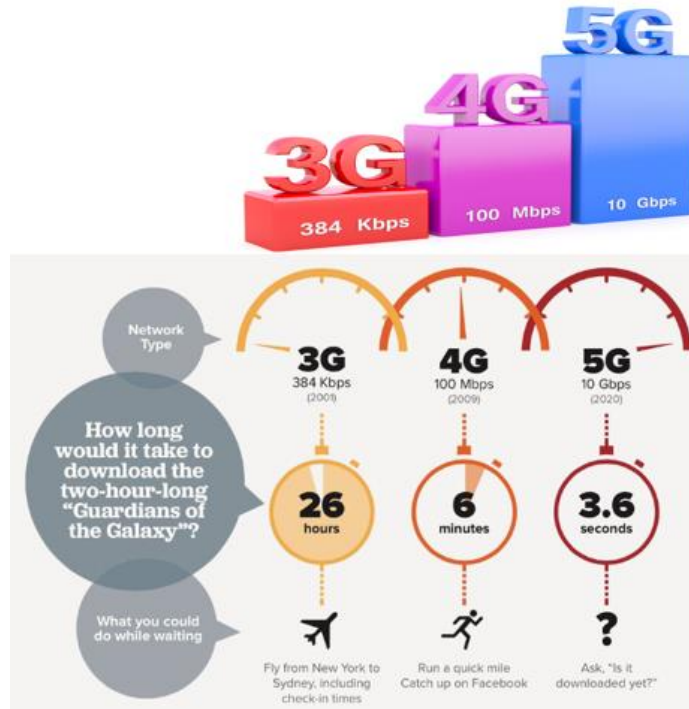
Figure 1   5G at a glance [3]

Also, the International Telecommunication Union (ITU) accepted a new 3G standard from China, i.e., TD-SCDMA (Time Division-Synchronous Code Division Multiple Access). Along with verbal communication, 3G systems provided data services, access to television/video, and new services like Global Roaming [1].

The Fourth Generation (4G) provides additional services like multi-media online newspapers and TV programs, and faster transfer data with LTE (Long Term Evolution) [1] as 4G technology. New access techniques such as OFDMA (Orthogonal Frequency Division Multiple Access) have made the communication structures more flexible. Time-frequency allocation is dynamic and adaptive MIMO (Multiple Input Multiple Output) techniques have improved data rate efficiently.

Table 1 summarizes the technology evolution and related and critical features.

Table 1 Technology evolution and related and critical features

Generation	Throughput	Standards	Starting	Features
1G	2 Kbps	AMPS, NMT, TACS	1980s	Analog Cellular Technology, Voice only
2G-2.5G	64kbps	TDMA, CDMA, GSM, GPRS	End of 1980s	Digital Narrow band circuit data, Packet
3G-3.5G	2Mbps	WCDMA	2000s	Digital Broadband Packet Data,
4G	100Mbps	LTE	2010s	Digital Broadband Packet, All IP
5G	10Gbps	NR, IOT	2020s	In Progress

1.2 5G Technologies

The expected 5G (fifth generation) concerns the next major phase of mobile telecommunications standard beyond the current 4G. 5G is considered as "beyond 2020 mobile communications technology", to bring new unique service capabilities to users and new industrial stakeholders.

As the fourth generation of wireless communication technology is already at its mature stage, in order to meet the ever-increasing demands of modern communication systems, 5G has been projected in the upcoming decade as next telecommunication standard beyond the current 4G and LTE standards.[2][4]

Data mobile traffic will be increased by an order of about one thousand times [1][2] as expected compared to what is experienced today. To meet this dramatic traffic growth [1][2], the fifth

Generation is being deployed to fulfil exceedingly rapid growth and promising commercial deployment in the next few years. On the aspect of standardization, since 2015, three major scenarios namely, enhanced Mobile Broadband (eMBB), ultra Reliable Low Latency Communication (uRLLC), and massive Machine Type Communications (mMTC), have been approved by the International Telecommunication Union (ITU) [2][4]. In July 2016, the Federal Communication Committee (FCC) adopted a new Upper Microwave Flexible Use Service. In December 2017, the first 5G new radio (NR) specifications were approved by 3Gpp, which marks a milestone for future large-scale trial experiments and wide commercial deployment [5].

On top of the standardization progress, as 5G heterogeneous networks become an immediate reality [4] [6], the application and usage scenarios will be largely enriched and thus, become more diverse and complicated than ever. In particular, there have been and will be more spectrum enhancement techniques such as, carrier aggregation (CA) and spectrum sharing paradigms represented by LTE Licensed Assisted Access (LTE-LAA). Implementing as many wireless standards and technologies on one single base station (BS) or user equipment (UE) is ultimately desired, but technically challenging and commercially expensive, considering that 5G cellular licensed high frequency bands such as 28, 37, and 39GHz, as well as WiFi mm-Wave bands (57-71GHz) pose very imminent challenges.

In fact, despite current limited hardware resources, slow growing battery performance, and strict form factor requirements [7] while realizing multi-function multi-standard tasks [8][9], 5G will be a key enabler for the Internet of Things (IoT) by providing Internet connection to a massive number of objects. Sensors and actuators will spread everywhere. Objects, users and their personal network, whether body-worn or in a household, will be producers and consumers of data. Future smart phones, drones, robots, wearable devices and other smart objects will create local networks, using a multitude of different access methods. 5G will also allow all these objects to connect independently from a specific available network infrastructure.

With its obvious advantages such as better data rate, wider channel bandwidth with NR (Next generation Radio Access Technology), better reliability, network scalability and flexibility, better efficiency and larger service in a crowded area, the 5G, which involves millimetre-wave (mm-

wave) frequencies, can be seen as the solution to the increasing demand for more bandwidth and higher data transfer rates. Indeed, Data rate improvement can be facilitated by different ways such as wideband antenna arrays with wide angle beam steering.

1.3 Research Motivations

As the demanding needs for 5G networks from technology evolution and the upcoming deployment of 5G from mobile communication service providers, this work focused on the design of planar array antennas operating at wide mm-Wave band 24.5-30.3 GHz for 5G mobile devices, with very small form factor to fulfill the size limitation in mobile devices, wideband operation bandwidth, high radiation efficiency, and relatively high gain.

Also, this thesis research performed a study on different antenna parameters related with overall radiation performance, i.e., antenna type, feeding technique, substrate selection including consideration of dielectric constant, loss tangent, thickness, etc. The outcome of this study generated a fundamentally design guide for mm-wave antenna arrays 5G of mobile communication systems.

The most common technologies used in radiofrequency circuits are microstrip. This technology has been studied and implemented during decades. It then compared with other approaches in order to choose the best solution for the field of 5G applications.

To broad operating bandwidth and improve realized gain, Franklin array concept was introduced to this design. The original idea comes from Franklin in 1924[10]. He first designed a Collinear Array (CoA) from a long wire that had λ/4 U-shaped sections to provide phase shift to maintain in-phase feeding of straight λ/2 parts of the wire (Figure 2). However, he faced the problem of resonant long wire antennas. In principle, the standing wave current distribution along a straight wire produces n radiation lobes of the same level, depending on the number n of half-wave antenna sections. By employing non-radiating quarter-wave stubs, Franklin converted the

original out-phase current distribution into an in-phased distribution of currents on collinear segments (solid red arrows in Figure 2), thus producing only one major radiation beam. A key advantage of such arrangement is the high gain of the antenna with the properties of series antenna array, whereas the simplicity of the single feeding point is maintained.

All antenna structures based on this principle, known as collinear arrays, are composed of in-phase fed radiating elements that lie in the straight line. Their radiation is typically broadside and perpendicular to the axis of collinear elements. Since Franklin's times, many collinear antenna structures have been proposed.

Solbach [11] designed a microstrip antenna derived from the Franklin's folded wire collinear idea, i.e., the Microstrip-Franklin antenna in 1982. Instead of U-shaped sections, he introduced small inductors to ensure phase shift (Figure 3). He started with the endeavor to suppress the radiation of the half-wavelength connecting lines situated between the patch radiators in the microstrip array. In comparison with Franklin, he proposed two 100Ω quarter-wave phasing stubs, producing a 180° phase shift between the terminals of the microstrip transmission lines. The stubs were designed symmetrically in order to maintain the parasitic discontinuity effects at the junction between the stub and the microstrip patch on the low levels. The currents on the phasing stubs are mutually opposite in direction so that the radiation produced by the stubs is cancelled.

Nevertheless, the electrical fringe fields of the terminating microstrip lines superimpose the phase in the slot between the lines. The resulting electric field in the slot was revealed as a prevailing source of radiation in the arrangement (see Figure 3). Such phasing stub can be described as a slot radiator embedded into the microstrip line and employing the radiators in question. It is possible to design the antenna array with a low spurious radiation and a low surface wave excitation [11].
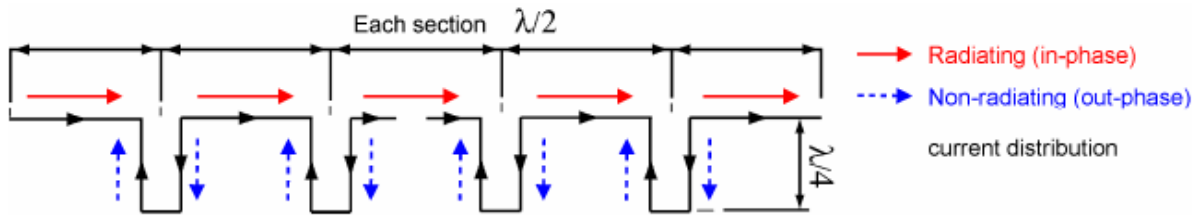
Figure 2 Franklin folded wire array
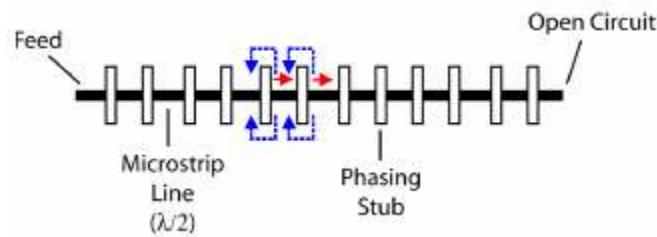
Figure 3 Improved Franklin array

The research in this thesis started with a normal circular patch antenna array and adopted the collinear planar antenna array concept to widen the operation bandwidth and reduce size.

1.4 Research Objectives

Due to the limited physical space [7] and coexistence with many other modules in the chassis of mobile devices e.g., camera, speaker, large LCD area, battery, microphone, etc., the first challenge for 5G mobile device antennas is to be of small form factor and low profile to fit in the chassis. Typically, the antenna location is limited to the edge areas.

Besides, to handshake with multiple bands in 5G networks, mobile antenna should be capable to operate over wideband bandwidth (around 21%). 28GHz band being the currently common band investigated by telecommunication providers such as Ericsson, Huawei and Nokia, this research

objective was to propose a design with wideband impedance bandwidth [13] compared to existing designs [16]-[32] to work better in mobile networks.

Second, there should be trade-offs between physical form factor, bandwidth and antenna gain. So achieving a gain above 10dBi compared to similar existing designs [18][19][20][21][26][28][31] was the second objective to reach. Below features are thus targeted for the design,

- Small size and lightweight for mobile terminals,
- Planar structure, easy to compact with other surfaces,
- S_{11} less than -10 dB over a wide frequency band (24.5–30.3 GHz),
- Relative high gain, peak gain greater than 10dB at 28 GHz,
- Easy to fabricate and low cost,

From the above, the main contribution of this thesis was to propose a Franklin antenna array with a small form factor for 5G mobile communication applications. Note that to the best of the authors' knowledge, it is the first time circular patches have been introduced into a Franklin array to achieve this design at 28GHz.

1.5 Thesis Outlines

The thesis consists of six chapters. Chapter 1 is an overall introduction about the technology evolution on mobile communication system, highlighting the trend on 5G demanding.

Chapter 2 serves as state-of-art study, which provides overview of the theory of antennas as well as recent antenna design for 5G mobile communication systems. Also, this chapter presents the requirements on critical antenna performance parameters, including gain, bandwidth, and radiation efficiency.

Chapter 3 focuses on radiation element design. The work based on circular patch antenna as radiation element, includes a parametric study to choose the best design for a 28 GHz antenna.

Substrate and feeding technique are also briefly covered. HFSS DDM simulations on circular array were performed to evaluate the proposed antenna far-field behaviour.

Chapter 4 introduces the collinear antenna array design based on Franklin theory, as a solution to address the bandwidth requirements and get a relatively higher gain from the antenna array. The proposed antenna array was simulated by HFSS for both near field and far field performance.

In Chapter 5, the proposed antenna was fabricated and tested showing good agreement with desired specifications.

Chapter 6 draws a general conclusion on the project and proposes different future work directions.

Chapter 2. State of the Art

2.1 Introduction to Antennas

An antenna plays a very important role in a radio system, transmitting and receiving radio waves. It is designed to transform guided electromagnetic waves present in a waveguide, feeder cable or transmission line into radiating free space waves, and vice versa, by reciprocity, collects power from passing electromagnetic waves. Thus, antennas should ensure radiation efficiency [8][9] [14]. Figure 4 shows how an antenna works as a transition region between guided and propagating waves.

Source   Transmission Line   Antenna   Radiated free-space wave
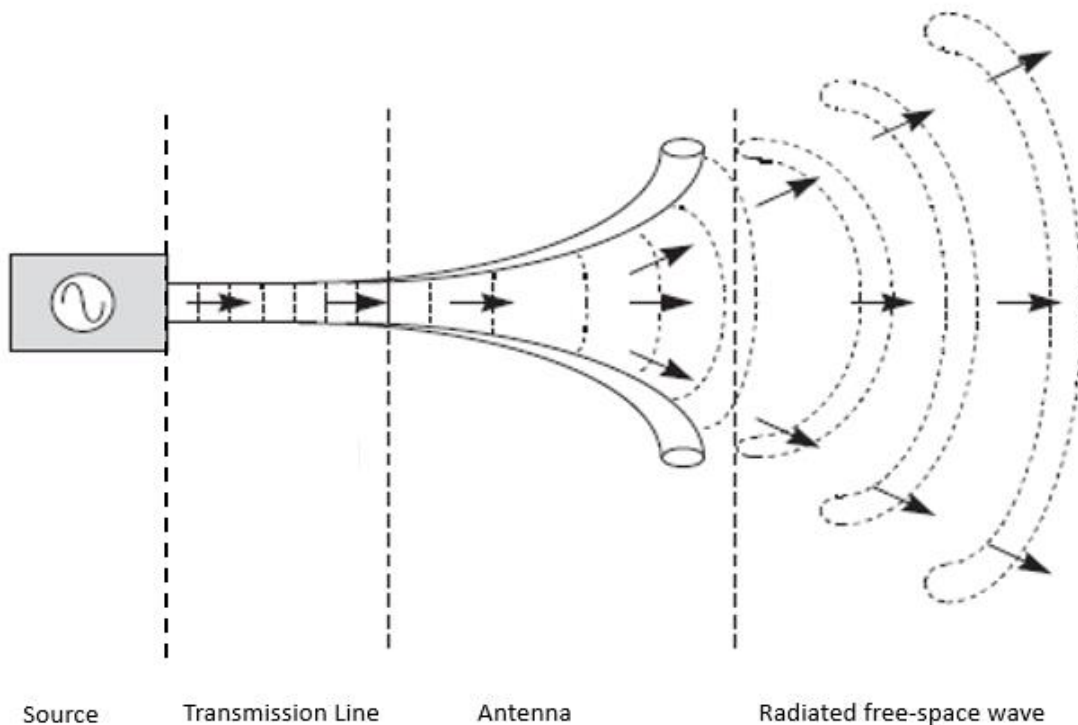
Figure 4 The antenna as a transition region between guided and propagating waves [9][14]

As in Figure 5, the antenna can be modeled in transmission line mode by a transmission-line electrical equivalent circuit. The source is represented by an ideal generator, connected to the

antenna with an impedance-controlled transmission line. The antenna resistance R_a is represented by two elements, the conduction and dielectric ohmic losses R_o and the radiation resistance R_r, while its reactance X_a is used to represent the imaginary part of the impedance associated with the antenna radiation, which models the energy stored in the near field of the antenna.
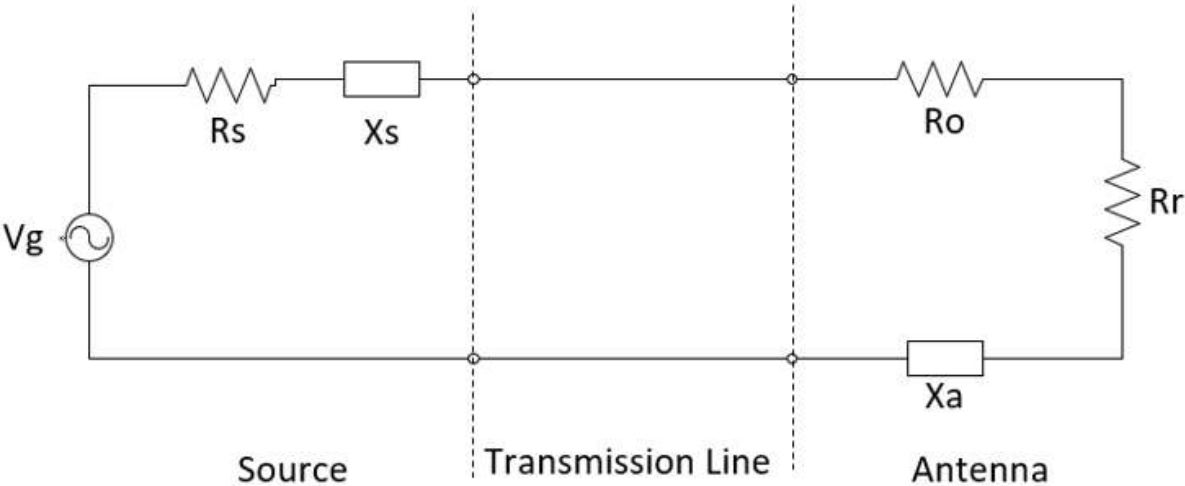
Figure 5 Transmission line equivalent circuit of antenna in transmitting mode [14]

Maxwell's equations predict that any time-varying orthogonally oriented electric or magnetic field produces the opposite field and forms an electromagnetic wave. The laws of electromagnetism that Maxwell put together are presented in Table 2.

Here E and H represent the respective electric and magnetic field intensities, D and B the respective electric and magnetic flux densities, P the volume change density and J the electric current density. The first two equations to predict electric and magnetic fields changes, the third and forth equations to predicate the electromagnetic waves propagation by introducing current displacement $\frac{\partial D}{\partial t}$.

Table 2 Maxwell equations

Differential Forms	Integral Forms	Notes
$\mathbf{\nabla} \cdot D = \rho_v$	$\oint_s \mathbf{D} \cdot d\mathbf{S} = \oint_V \rho_v \cdot dv$	Gauss's law
$\mathbf{\nabla} \cdot B = 0$	$\oint_s \mathbf{B} \cdot d\mathbf{S} = 0$	Nonexistence of isolated magnetic charge
$\mathbf{\nabla} \times \mathbf{E} = -\dfrac{\partial B}{\partial t}$	$\oint_L \mathbf{E} \cdot dI = -\dfrac{\partial}{\partial t}\int_S \mathbf{B} \cdot d\mathbf{S}$	Faraday's Law
$\mathbf{\nabla} \times \mathbf{H} = J + \dfrac{\partial D}{\partial t}$	$\oint_H \mathbf{H} \cdot dI = \int_S (J + \dfrac{\partial D}{\partial t}) \cdot d\mathbf{S}$	Ampere's Law

The first challenge to 5G systems is the high operating frequency, i.e., mm-wave bands, to avoid the already very crowed current 3-4G spectrum while benefit the availability of a wide portion of unused bandwidths in mm-wave bands. However, mm-waves have very different propagation conditions, atmospheric absorption, and hardware constraints compared to centimeter-waves. These challenges could be compensated by using beamforming and a larger antenna array [15]. It is widely accepted that the mm-wave band must be used with a limited cell radius (<100 m) to minimize high path loss. There will be approximately 23 and 31 dB of extra path loss when moving the operating frequency from 2 GHz to 28 GHz or 70 GHz, respectively [15].

A second challenge is signal attenuation at high frequency bands. This is a serious issue because it limits signal propagation. The oxygen molecule absorbs electromagnetic energy at around 60 GHz; therefore, the free-licensed band from 57–64 GHz has high oxygen absorption with attenuation of approximately 15 dB/km. Furthermore, water vapor absorbs electromagnetic energy at 164–200 GHz with even higher attenuation [15].

A third challenge is that millimetre-wave signals penetrate solid materials with very high losses (if they can penetrate such materials), which makes them too sensitive to obstacles such as buildings. High levels of attenuation could limit the use of millimetre-wave communication from

outdoor cells to only outdoor receivers. Indoor coverage would thus be provided by indoor millimetre-wave small cells or Wi-Fi solutions.

Unused or underutilized Local Multipoint Distribution Service (LMDS) broadband spectrum exists at 28 GHz, and given the low atmospheric absorption, the spectrum at 28 GHz has very comparable free space path loss as today's 1-2 GHz cellular bands as stated in [15]. In addition, rain attenuation and oxygen loss do not significantly increase at 28 GHz, and, in fact, may offer better propagation conditions as compared to today's cellular networks when one considers the availability of high gain adaptive antennas and cell sizes in the order of 200 meters [15].

2.2   Literature Review- Antenna for 5G

Recently, several mm-wave planar antenna arrays have been studied and designed for 5G mobile communication systems (Table 3).

In [11], phasing stubs have been employed to achieve a co-phase current distribution in microstrip rectangular patch arrays. This technique, originally proposed by Franklin for resonant long wire antennas, avoids spurious radiation from half-wavelength connecting transmission lines as used in conventional patch antenna arrays. A slot radiator model has been derived to describe the basic radiation mechanism of the resultant new type of antenna. The design of a 13-element resonant array for 12 GHz is also discussed in Table 3.

In [16], a 16-element wideband antenna has been proposed with a Butler matrix feed network fabricated on a low-cost laminate with area size 47x35x0.13 mm^3. The patch antenna has a broad radiation pattern for wide-angle beam steering and allows the simultaneous operation with two orthogonal linear polarizations. A combination of two separated Butler matrices provides independent beam steering for both polarizations in the wide operating band of 27-33.7 GHz.

In [17], a 28GHz 4x4 antenna array has been fabricated for 5G base station applications, with capability to be connected to a RF front-end allowing beamforming. The dimensions of the design are 78.5x42 mm^2 with 1.5 GHz operating bandwidth and a reported achievable gain of 18 dBi.

The work in [18] presented a novel hybrid antenna module concept at millimeter-waves to realize spherical beam steering coverage that is structurally and systematically compatible with current cellular devices. The hybrid antenna module concept coherently combines two existing concepts - the AiP (Antenna-in-Package) and the AoD (Antenna-on-Display) to steer the antenna main lobe in the end-fire and broadside direction. A compact end-fire antenna array (AiP) and a fully optically transparent antenna array (AoD) achieve impedance bandwidth (2:1 VSWR) of 1.67 GHz and 0.85 GHz respectively at 28 GHz. Investigation in the far-field ascertains that the 4-element end-fire AiP and the 16-element broadside AoD exhibit a gain of 9.2 dBi and 12.8 dBi in the θ = 90° and θ = 0° plane, respectively.

A compact antenna array design utilizing the concept of connected antenna arrays (CAA) has been discussed in [19]. CAA presents wideband antenna responses that can be very suitable to mm-wave applications as well as provides more compact antenna sizes that can be integrated within mobile terminals compared to conventional ones. A 100x60x0.76 mm^3 slot-based CAA has been proposed for standard mobile handset size terminals that includes 4G (1.8-3.1 GHz) and 5G mm-wave (27.2- 28.5 GHz) antenna systems. The reported gain for 5G antenna is about 10 dBi.

In [20], a miniaturized Dielectric Resonator Antenna (DRA) array of 3D-coverage for 5G mobile terminal applications is presented. Two subarrays placed at both ends of the substrate have been used to realize a 3D-coverage beam scan with a less linear array. Here, the subarray has 8 antenna elements and works as a phased array, so that these two subarrays are responsible for radiation in two different regions. Also, each antenna element is a miniaturized DRA whose size is reduced to be half of the size of the original antenna by loading the metal sheet. The simulated results show that the proposed design covers over 5 GHz bandwidth in the band of 26 GHz, with an area of 60×120 mm^2 and a height of 2mm. Achieved gain was about 10 dBi.

In [21], a millimetre-wave flexible antenna for 5G wireless applications is reported. The antenna geometry comprises of a T-shaped patch integrated with symmetrically designed slot arrangements. The defected ground structure (DGS) concept has been utilised for bandwidth enhancement and a coplanar waveguide (CPW)-fed slotted monopole antenna embedded within an aperture cut inside the ground plane. The measurements of the inkjet-printed antenna prototype depict an impedance bandwidth of 26–40 GHz, consistent omnidirectional radiation pattern, and a peak gain of 7.44 dBi at 39 GHz.

In [22], a novel capacitive coupled patch antenna array design was positioned in the mobile phone chassis as a set of 4 sub-arrays each with 12 antenna elements to provide high gain around 27 dBi with each sub-array providing 90 degree coverage. The antenna array covers the frequency range of 24-28 GHz, a promising band for future 5G based smartphone services. The antenna has 12 radiation elements of 3.7x3.25 mm each with a separation between the 12 elements of 6.3mm.

In [23], a novel mm-wave phased array antenna for whole metal covered 5G mobile handset has been proposed. It consists of eight rotated slot antenna elements arranged on the upper frame of the metal-body. The proposed antenna operates between 27.1 and 28.6 GHz and has a hemi-spherical beam coverage suitable for 5G mobile communication. The 138x67.1x7.1mm^3 antenna was configured on the metal body of the handset top section with a gain up to 13.7dBi.

In [26], a 12x28.2x0.4mm^3 compact, flexible and wideband mm-wave Franklin antenna array was designed at for upcoming 5G applications. Measurements showed that the designed array covers the band 24.6–30 GHz with a simulated gain of 8.3dBi at 28 GHz.

In [28], a modified uniplanar compact Franklin antenna array was designed for future 5G communications. The proposed antenna is composed of five mm-wave hexagonal antennas forming an array 9.8x27.4x0.5mm^3. The operation frequency range covers the 24-30 GHz band with a maximum gain of 10.7 dB at 24GHz.

In [29], a novel low-cost, high-gain millimeter-wave antenna has been introduced. The antenna of 96.5x102x0.508mm^3 is a 6×5 proximity-coupled planar array suitable for 5G cellular

applications. The reported gain is 21 dBi over a bandwidth of 27.5–28.5 GHz. It also exhibits an impedance bandwidth of 9.8% from 26.04 to 28.78 GHz.

In [30], a phased array antenna was designed at millimeter-wave frequency bands for future 5G based smartphone applications. The proposed antenna is a novel open slot-PIFA antenna. The antenna array covers a frequency range of 26-32 GHz. The 8-element antenna array exhibits a maximum gain of 13 dBi. It utilizes the cellphone chassis as ground, with a height of 1.6mm. The pattern can be steered by varying the phase shift at each antenna element.

In [31], a novel modified compact broadband antipodal Vivaldi antenna (AVA) array for future 5G communication systems has been discussed. The proposed structure of $28.823\times60\times0.787\text{mm}^3$ consists of 8 antenna elements that are fed by a 1-to-8 power divider. Multiple notch structures were added on the ground plane. Impedance bandwidth was extended slightly from 24.65–28.5 GHz to 24.55–28.5 GHz, and the gain improved simultaneously. Measurement results showed a gain of 6.96–11.32 dB in the operating frequency band.

In [32], the design of an 8-element microstrip patch antenna (MPA) array for dual-band 5G communications is discussed. The proposed antenna array is compact of size $16\times16\text{mm}^2$. The dual-band responses at 28 and 38 GHz have been achieved by etching an inverted U-shaped slot from the main radiator. Coupling between elements was about -10dB @28G and -5.5dB @39.95GHz, with a narrow bandwidth at each resonant frequency range.

Table 3 summarizes the recent mm-wave antenna designs.

Table 3 Literature review of recent mm-wave antenna designs

Ref.	Type	Volume (in mm)	substrate	f (GHz)	bandwidth	Gain (dBi)	Year	Notes
[11]	1x13	Not shown in paper	RT/Duroid 5870	12G			1982	Phasing stub introduced
[16]	4x4 patch sub array	47x35x0.5	RO3003	28	27-33.7,		2017	Butler feed network
[17]	4x 4 patch sub array	78.5x42 (no thickness data in paper)	RO4350b	28	1.5G	11.5	2018	
[18]	1x16 patch array	15.4x92.8 (no thickness data in paper)	LTCC, 8 layers	28	1.67	9.2 @θ=0 12.8@θ=90	2018	Feeding network included
[19]	Slot CAA	60x100x0.76	RO4350B	27.2- 28.5		Approximate peak 10dBi 5G antenna	2018	Feeding network on bottom plane, Mobile Terminals
[20]	2X8 DRA array	60x120X2(DRA)	FR4 Substrate 1mm	23.2 -28.6		Approximate peak 10.5dBi	2018	DRA hight 2mm, feed network not presented, Mobile Terminals

[21]	T shape patch	16x16 (no thickness data in paper)	PET	26–40		7.44@39G >4dBi over frequency range	2018	wearable applications
[22]	4x12 patch array	(not shown in paper)	RT5880	24-28		Peak gain 27dBi Each array 6.26dBi	2017	Feed network not presented
[23]	1x8 slot array	17.28x67.1x7.1		27.1 -28.6		Peak 12 to 13.7	2017	Feed network not presented. Mobile Phone
[26]	1x6 Rectangular patch	12x28.2x0.4	PET film	28G	24.6-30	8.3dBi @28GHz	2017	With phasing stub
[28]	1x5 Hexagon patch	9.8x27.4x0.5	RO3003	28G	24-30	10.7dB@24GHz	2017	With phasing stub

Ref	Array	Dimensions	Substrate	Freq	Bandwidth	Gain	Year	Notes
[29]	6x5 sub array	96.5x102x0.508	two stacked Taconic TLY-5 substrates	28G	27.5-28.5	21dBi	2018	proximity-coupled microstrip planar antenna
[30]	1x8	150 × 74x1.6 handset ground	RT5880	28	26-32	13dBi	2017	slot-PIFA
[31]	1x8 AVA array	28.823x60x0.787	RT5880	28	24.75-28.5	6.96-11.32 dBi	2018	AVA
[32]	8 elements patch array	16x16 (no thickness data in paper)	FR4	28 G 39 G	Narrow bandwidth	15.6@ 28 15@39.95	2017	Feeding not presented, Elements Coupling need monitor

2.3 Requirements for mobile antennas

Mobile devices, such as cell phones or wearable devices, typically require antenna to be of low profile, small form factor [7], good radiation capability, and wide operating frequency range to hand shaking between communication network sectors.

Nowadays, the physical size of mobile devices is getting smaller and thinner to fulfill customers' appearance requirements, meanwhile such device needs consist of many subsystems to achieve variable useful functions. Therefore, the antennas should be designed as small as possible. However, small size creates challenges as other requirements cannot be neglected.

Also, to bring the design in reality commercial uses, mobile device antennas should be designed to be easily manufactured. Furthermore, the antenna design is useless if it is not robust against mechanical damages or cannot be mass produced at reasonable costs.

2.3.1 Operating Frequency Bandwidth

Bandwidth can be described as a percentage from a center frequency or a range from lower to upper limit, where different parameters (e.g. gain, efficiency, matching) are still at acceptable level. Since antenna characteristics vary from not-at-all frequency dependent to critically affected by frequency, bandwidth cannot be clearly characterized. Usually it is specified separately for each application.

Bandwidth can be defined as pattern or impedance bandwidths. Pattern bandwidth is associated with gain, side lobe level, and beam width, while impedance bandwidth relates to input impedance, matching, and radiation efficiency.

Mobile terminals require a wide operational bandwidth, and small antennas are typically providing narrow bandwidth. As explained in the previous sections, there is a trade-off between

bandwidth and matching level, which can be solved by finding a good compromise between them. Bandwidth can be increased at the expense of antenna size or efficiency [19]. Multi-resonant matching circuits provide an efficient way to improve bandwidth. Adding resonators can double or triple the available bandwidth, but at the same time, the complexity and losses of the whole system increase. Besides multiple resonators, wider bandwidth can be achieved with frequency tunable matching circuits. If the operational band can be split into sub-bands, that are not simultaneously needed, digitally tunable capacitors (DTC) can be used. As well as with multi-resonators, using DTCs also increases complexity and losses in the system. The third way to increase bandwidth is to sacrifice efficiency. Accepting worse matching level might nearly double the bandwidth and efficiency would weaken mainly at the borders of the frequency band [19].

The impedance Bandwidth indicates the bandwidth for which the antenna is sufficiently matched to its transmission feed line, such that the input incident signal power loss due to reflection will be less than 10%. The impedance presented by the antenna at its input terminal changes with frequency. If this impedance is not the same as that of the antenna, then an impedance mismatch results and maximum power transfer will not occur. Impedance bandwidth indicates the bandwidth for which the antenna is sufficiently matched to its input transmission line such that 10% or less of the incident signal is lost due to reflections. Impedance bandwidth measurements include the characterization of the Voltage Standing Wave Ratio (VSWR) and return loss throughout the band of interest.

Reflection Coefficient

The reflection coefficient Γ is defined as the ratio of the reflected wave to the incident wave in (2.1),

$$\Gamma = \frac{Z_{in} - Z_o}{Z_{in} + Z_o} \qquad (2.1)$$

where Z_{in} is the antenna input impedance and Z_o the transmission line characteristic impedance.

VSWR

The voltage standing wave ratio (VSWR) is the ratio of the maximum to minimum voltage on a transmission line and is defined as (2.2),

$$VSWR = \frac{1 + |\Gamma|}{1 - |\Gamma|} \qquad (2.2)$$

RL

Return loss *RL* is a measure of the difference between the power input to and the power reflected from a discontinuity in a transmission circuit. It is often expressed as the ratio in decibels of the power incident on the antenna terminal to the power reflected from the terminal at a particular frequency or band of frequencies. It can be defined as

$$RL = -20 log_{10}|\Gamma| \qquad (2.3)$$

The return loss is a measure of the reflected power due to the impedance mismatch of the antenna and is defined in terms of reflection coefficient

$$RL(dB) = 10 log_{10}\left(\frac{P_{in}}{P_{ref}}\right) = -10 \log|S_{11}|^2 \qquad (2.4)$$

where *RL* (dB) is the return loss in dB, *Pin* is the incident power on the antenna and *Pref* is the reflected power to the source.

ML

The mismatch loss (*ML*) represents the fraction of power that is radiated due to the impedance mismatch between the antenna terminal and the transmission line.

It is defined as (2.5):

$$ML = 10log_{10}(1 - |\Gamma|^2) \qquad (2.5)$$

The bandwidth of an antenna can be considered to be the range of frequencies, on either side of the centre frequency, where the antenna characteristics are within an acceptable value of those at the centre frequency. Usually, in wireless communications, the antenna is required to provide a return loss less than -10 dB over its frequency bandwidth. The bandwidth specifications are set in each case to meet the needs of the particular application. For narrowband antennas, the impedance bandwidth is expressed as a percentage of the frequency difference (upper minus lower) over the centre frequency of the bandwidth, which is given as (2.6),

$$BW = \frac{f_h - f_l}{f_c} * 100\% \qquad (2.6)$$

A good impedance match typically indicate by $S_{11} \leq$ -10dB, VSWR $\leq$ 2, and $\Gamma \leq$ 0.3162 [9][14]

2.3.2 Gain

Gain is an indicator of the ability of the antenna to direct the input power into radiation. It is measured at the peak radiation intensity, usually monitored in a particular direction. Power density S radiated by an isotropic antenna with input power Pin at a distance R, and is proportional to $1/R^2$, while, E is proportional to $1/R$. It is convenient to define radiation intensity to remove the $1/R^2$ dependence, Radiation intensity U depends only on the direction of radiation and remains the same at all distances.

$$S(\theta, \varphi) = \frac{P_{in}G(\theta, \varphi)}{4\pi R^2} \qquad (2.7)$$

and

$$U(\theta, \phi) = \frac{P_{in}G(\theta, \phi)}{4\pi} \qquad (2.8)$$

Gain is a parameter closely associated with the directivity of an antenna. The gain takes into consideration any losses within the antenna. Antenna gain is defined as (2.9):

$$G(\theta, \phi) = \frac{4\pi U(\theta, \phi)}{P_{in}} \qquad (2.9)$$

where P_{in} is the net power accepted by the antenna at its input terminals from the connected transmitter (in transmit mode) or the power available at the antenna input terminals (in receive mode). The power (P_{in}) at the antenna input terminals is related to the antenna radiated power (P_r) by (2.10):

$$P_r = e_{rad}P_{in} \qquad (2.10)$$

where e_{rad} is the antenna radiation efficiency. The antenna radiation efficiency is a measure of how much of the power entering the antenna is radiated and it accounts for conduction and dielectric losses in the antenna. By comparing the above three equations, the gain can be related to directivity by (2.11):

$$G = e_{rad}D \qquad (2.11)$$

Gain does not include impedance mismatch losses or polarization mismatch losses.

2.3.3 Efficiency

Radiation efficiency is a very important figure of merit for mobile devices, which can indicate the antenna behaviour regarding the proportion of input power transformed into radiation to free space. In general, an efficiency factor is the ratio of wanted power to total power supplied, so antenna efficiency can be defined as the ratio between the radiated power (P_r) to the input power (P_{in}). Figure 6 shows the reference points for input and output power. Total antenna efficiency is described in (2.12)

$$e_a = e_{ref}e_{rad} \qquad (2.12)$$

where, e_{ref} is the reflection efficiency and e_{rad} the radiation efficiency. The overall antenna efficiency includes losses due to an impedance mismatch and the conduction and dielectric loss caused by the input terminals of the antenna. If the antenna input port has a reflection coefficient of Γ, then the antenna efficiency is given by (2.13):

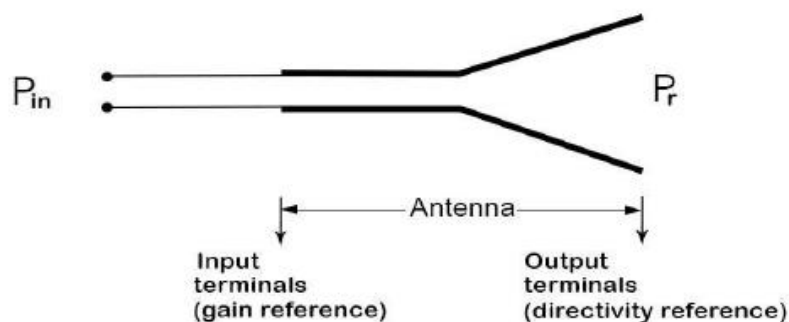$$e_a = \frac{P_r}{P_{in}} = \frac{P_r}{P_r + P_o} = (1 - |\Gamma|^2)e_{rad} \quad (2.13)$$

Figure 6 Antenna reference terminals [14]

with,

P_r = power radiated

P_o = power dissipated in ohmic losses on the antenna

$P_{in} = P_r + P_o$ = input power or power accepted by the antenna

Also, antenna efficiency can be derived from the surface integral of the radiation intensity over the radiation sphere divided by the input power, i.e., a measure of the relative power radiated by the antenna, or the antenna efficiency

$$e_a = \frac{P_r}{P_{in}} = \int_0^{2\pi} \int_0^{\pi} \frac{G(\theta, \phi)}{4\pi} \sin \theta \, d\theta d\phi \quad (2.14)$$

Poor impedance matching or insertion loss from the antenna can reduce the radiated power, leading to poor efficiency.

2.3.4 Radiation Pattern

The radiation pattern is a graphical representation of the radiation properties of an antenna as a function of space coordinates. It is usually specified in the far field region of the antenna (a region far enough away from the antenna where the angular field distribution is essentially independent of distance). The most useful radiation pattern is the 3D spatial distribution of the radiated energy as a function of an observer's position along a constant radius.

For a linearly polarised antenna, its performance is often described in terms of its *E*-plane and *H*-plane patterns.

- The *E*-plane is defined as the plane containing the electric field vector and the direction of maximum radiation.

- The *H*-plane is defined as the plane containing the magnetic field vector and the direction of maximum radiation.

There is always a trade-off between directivity and gain. Due to the randomly changing orientation of the mobile devices, an omnidirectional pattern in azimuth is desirable, as well as wide beam width. However, the precise pattern is not that important given the propagation environment and the proximity of the user.

2.3.5 Directivity

Directivity is a measure of the amount of energy concentrated in the main beam of an antenna pattern. It can also be defined for an arbitrary direction $D(\theta, \phi)$ as the radiation intensity divided by the average radiation intensity. The directivity of an antenna is equal to the ratio of the radiation intensity in a given direction over that of an isotropic source. The radiation intensity (U_o) of an isotropic source is, by definition, independent of spherical angles θ and ϕ, and is equal to the radiated power averaged over the entire solid angle of 4π. The maximum directivity can be expressed as (2.15),

$$D(\theta, \phi) = \frac{U(\theta, \phi)}{U_o} = \frac{4\pi U(\theta, \phi)}{P_{rad}} \qquad (2.15)$$

where,

$$U_o = \frac{P_{rad}}{4\pi} \qquad (2.16)$$

and the Power Intensity U in a given direction is a far-field parameter defined as the power radiated from an antenna per unit solid angle, and expressed as (2.17),

$$U(\theta, \phi) = r^2 W_{rad}(r, \theta, \phi) \qquad (2.17)$$

2.3.6 Polarization

Polarization is an important characteristic of antennas. Transmitting and receiving antennas should be aligned according to their polarization to enhance reception.

The polarization of an electromagnetic wave describes the time-varying direction and relative magnitude of the electric-field vector. If the time-varying electric field is represented by a vector, the polarization of the wave can be thought of as the locus traced by the tip of this vector in time, at a fixed position in space. The sense of polarization is defined as being observed in the direction of propagation. The polarization of an antenna is defined as being the same as the polarization of a wave transmitted by that antenna. In the most general case, a plane wave will have an elliptical polarization, as shown in Figure 7. In other words, at a fixed point in space, the magnitude of the electric field will trace out an ellipse. Defining the major axis of the ellipse as *a* and the minor axis as *b*, the ratio of the two is known as the axial ratio (*AR = a/b*).
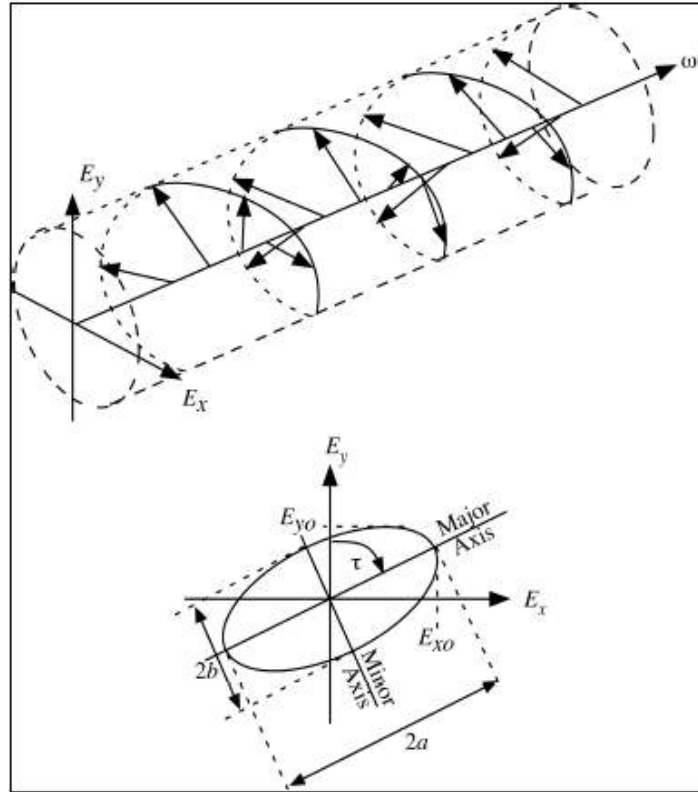
Figure 7 Electromagnetic wave polarization [14]

There are two special cases [14],

- $b = 0$, ($AR = \infty$), the wave is said to be linearly polarized.

- $a = b$ ($AR = 1$), the wave is said to be circularly polarized. For circular polarization, the sense of polarization can be either clockwise (right-hand) or counter clockwise (left-hand) as observed along the direction of propagation.

2.4 Typical Antenna types for mobile devices

Mobile antennas operate on a wide frequency range in a small mechanical size. To achieve the small size and wide frequency band, below antenna types were analyzed and compared.

2.4.1 Dipoles and Monopoles

Dipole antennas are widely used because of their simple structure, ease of fabrication in mass production, high efficiency, and omnidirectional radiation pattern.

They are resonating antennas, which operational frequency depends on their length. The most widely used one is the half-wave dipole. By nature, dipoles are narrowband antennas, but there are trade-offs that designers can use to widen bandwidth (e.g., by using larger wire width). However, even if dipoles are electrically small, they are usually physically large structures [8][14], which is not favorable for mobile handhelds and other wearable devices. Also, dipoles being physically too large for mobile applications, mobile antennas are surrounded by very nearby modules in a small chassis, which will impact the antenna performance. Normally, these objects are ground planes that are large compared to the antenna. Conductive ground planes affect antenna's performance, especially impedance and radiation pattern.

Alternatively, monopole antennas are designed to operate in the presence of a ground plane. A monopole is basically a dipole cut in half and fed against the ground plane. Monopole impedance is half of that of a dipole, and accordingly, the radiated power is half of that of a dipole with the same current, as the radiation occurs only in one hemisphere [33]-[37]. This yields to lower average radiation intensity, which gives higher directivity. Operational frequency of a monopole naturally depends on the length of the antenna, similarly to dipoles, but their smaller size makes monopoles potentially suitable for mobile devices [8][9].

2.4.2 Loops and slots

Loop antennas are another type of simple wire antennas that can take various forms such square, circular and triangular. They are versatile and inexpensive, and widely used in short-wave communication applications as well as a substitute for monopoles due to their resilience against noise. Loop antennas are usually classified into two categories namely, electrically small (circumference < $\lambda/10$) and electrically large (circumference on the order of λ). Electrically small loop antenna has a poor radiation resistance, which is the reason why they are not commonly used in transmission. The radiation resistance can be improved by increasing the number of turns, which, however, also increases losses by nature. Radiation pattern of a loop antenna equals to that of a magnetic dipole [14][8].

Slot antennas are variants of loops. Usually an antenna of this type is a slot in a ground plane. The electric field distribution of a slot is equal to a similar dipole, and the field is directed along the normal of the slot elsewhere in its surface except the slot region itself [26]. Slots can be fed from a waveguide, which makes these antennas popular for vehicles moving at high speeds. Typically, slots operate on a narrow band, which makes them not so popular choice for mobile devices.

2.4.3 Planar antennas

Traditional dipole or monopole antennas are usually too large to fit in the limited chassis space of mobile devices. However, monopoles can easily be modified to accommodate the size requirements by bending the wire antenna to the form structures of inverted L-antennas (ILA) [14][65]. Replacing wires with a strip changes the structure to a planar inverted L-antenna (PILA), which results in wider bandwidth. PILAs are, however, sensitive to changes in height (h) or length (l) of the antenna. Height lower than $0.1\lambda_O$ is considered critical since above that the antenna is

rather top loaded monopole than a PILA. Also, antenna's matching improves if h/l ratio is greater than 4/3 [65].

By adding a parasitic grounding strip near the feed point to form a planar inverted F-antenna (PIFA), the antenna matching can be effectively maintained. Even though the overall dimensions required for good performance, especially at low frequencies, might seem quite large, PIFAs and PILAs are suitable for cellular phones due to their low-profile structure and large achievable bandwidth. Planar antennas have been used widely in mobile phones since their release due to the large modifying possibilities of the structure.

2.4.4 Microstrip antennas

Microstrip antennas are attractive in modern mobile devices. The Microstrip antenna (MSA) can be printed on thin and flexible substrates, which offers the possibility to fit in mobile devices space and conformable to various mounting surfaces and structures. Another potential advantage of microstrip antennas is that they can be integrated in microwave integrated circuits, to be off-shelf designs to shorten design time and lower design costs, and of course to save physical space [14].

Microstrips have advantages such as radiating with a broad beam broadside to the patch, while the ground plane prevents the formation of back lobes. However, the patch antenna has also a narrow bandwidth and after fabrication, cannot be re-adjusted easily.

To widen the operation bandwidth, some techniques have been proposed [16], [20]-[31], e.g., feeding techniques and phasing stubs. For instance, the collinear phasing stub can improve the patch antenna bandwidth and achieve relative higher gain, which makes the patch antenna suitable for mobile device design.

2.4.5 Bowtie antenna

The radiation pattern of a Bowtie antenna is similar to that of the dipole antenna, with a vertical polarization, and specified solely by the angle between the two metal pieces. The antenna feed is at the center of the antenna, which is the radio positive and negative terminals connect with antenna. Theoretically, if the bowtie antenna is infinitely long in both directions, it would have an infinite bandwidth because the antenna looks the same at all wavelengths. When clipping the bowtie antenna arm to a certain length, the structure can be wideband [39][40].

Bowtie antennas can achieve wideband operating frequency. However, they require baluns to sustain their performance. In [41]-[43], Marchand baluns have been employed to differentially feed dipole array elements and built-in as a part of the impedance matching network. Besides, because Bowtie antenna excitation feeding points are in the middle of the antenna, they are not feasible to build as linear feeding arrays, which indicates that if the bowtie antenna has to be applied in 5G arrays, the feeding network should be designed as reported in [44], then extra board space will be taken in the application chassis, thus increasing design complexity as well. So bowtie antennas cannot be selected for this work.

2.4.6 Log periodic antenna

By adding the arms in a log periodic manner, bowtie antennas bandwidth can be further increased, including Log Periodic Dipole Array (LDPA), Log Periodic Toothed antenna and Log Periodic Trapezoidal antenna with different arms design methodologies [45]. Even Log periodic antenna can offer wideband operating features, this kind of design needs an accurate control of the arms radius and angles, which is difficult to realize on 5G applications when wavelength getting shorter to millimetre range. Besides, similar with Bowtie antennas, Log Periodic antennas need to implement the feed point in the middle as well as baluns in their feeding structure.

To the best of the author's knowledge, there is no design of LDPA, Log Periodic Toothed antennas and Log Period Trapezoidal antennas reported in the literature for 5G mm-wave applications. Furthermore, based on the manufacturing complexity and feeding network board space, Log Periodic antennas cannot be suitable for this work as well.

2.4.7 Leak Wave Antenna (LWA)

Leak wave antennas are collinear antenna arrays fed serially at edges. One of the most important features of leak wave antennas is that they change the main beam directions by changing the working frequencies, so that different angles data scanning can be achieved. Leak wave antennas have many similar features as the Franklin antenna array and they are widely applied in many communication systems, radars and millimeter wave imaging systems: low cost, simple structure, lightweight, easy to manufacture and integrate into other microwave circuits … [46]. However, the original leak wave antenna operating bandwidth is relatively narrow. To widen impedance bandwidth, solutions such as all-pass delay lines [46]-[50] can be integrated. However, they increase the fabrication complexity. A recent study on improving the leaky wave antenna impedance bandwidth was done in [51] by implement Complementary Microstrip-Slot line Stubs which was a quite close idea as the phasing stub in Franklin arrays.

Thus, Instead LWA antennas, the Franklin array was proposed in this work to achieve the advantages of LWA and avoid the disadvantage of narrow impedance bandwidth.

2.4.8 Substrate Integrated Waveguide (SIW)

Substrate Integrated Waveguide (SIW) technology is for combining the advantages of both the conventional microwave and planar (microstrip) components. The SIW can be described as a planar structure such that the top metal layer and the bottom ground layer are connected via

metallic cylinders called via holes in the form of two periodic rows. Therefore, SIW components possess specifications like small size, depressed weight, and minimal cost since the making and reliability are enhanced. Moreover, the planar shape of the waveguide allows integrating SIW-based components with other PCB components on the same board.

SIW arrays have proven to yield high impedance bandwidths. However, they suffer from excessively large form factors [52][52][53]. Besides, multi-layer PCB technology or low temperature co-fired ceramic (LTCC) needs to be exploited to realize air cavities [54] or thick substrates [55][56], resulting in a significant increase of complexity and manufacturing cost. Moreover, stacked patch antennas demonstrate large impedance bandwidths, which add crosstalk risks due to the integrated structure fairly low antenna/platform isolation, making SIW technology a potential candidate for 5G mobile applications but not viable choice due to high-density integration product structure.

2.5 Conclusion

General antenna parameters were studied and different antenna technologies were compared in this chapter 2. Meanwhile, the latest 5G antenna designs posted in the period 2017-2019 were reviewed as well to generate the comparable design target for this research. To consider the overall radiation performance, size limitation and conformal requirements for 5G mobile devices, the proposed antenna will be designed with microstrip antenna technology. The detailed circular radiation element design and modeling will be described in the next chapter.

Chapter 3. Radiating Element Design

3.1 Patch antenna for mobile devices

A microstrip patch antenna consists of a metallic patch placed on an electrically thin, but large, grounded substrate. Microstrip antennas offer numerous attractive features [14]:

- Low profile, conformable to various surfaces and light weight.
- Suitable for mass production and cost-effective.
- Compatible with active component design such as smart antenna systems.
- Very Versatile as below listed features:
  - Linear or circular polarization.
  - Can operate over a large range of frequencies (0.5 - 60 GHz).
  - Easily to form linear or planar arrays.
  - Easy impedance control.

Patch antennas can be designed with numerous shapes, including rectangular, circular, triangular, ring, disc sector, or annular.

Microstrip patch antennas have been widely used because of their good characteristics. However, the signal propagation path loss will challenge the design of mm-wave antennas [15]. A typical microstrip transmission line is shown in Figure 8.
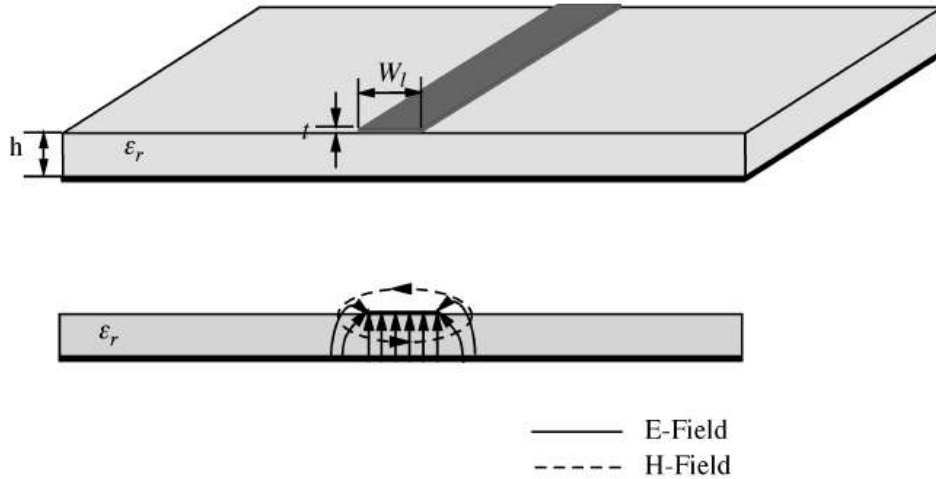
Figure 8 Microstrip Transmission Line

The inhomogeneous configuration of the microstrip line (with air above and dielectric below) can be converted to a homogenous configuration, as shown in Figure 9, by replacing the air and substrate with a new medium with an effective dielectric constant (ε_e). The effective dielectric constant will have a range of values between $1 < \varepsilon_e < \varepsilon_r$, and is also function of frequency.
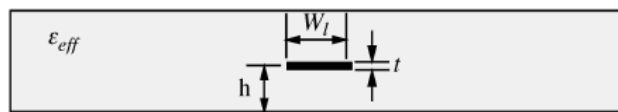

Figure 9 Equivalent Homogeneous field

3.2 Patch Antenna using Rogers Substrate

The first step in designing a microstrip patch antenna is to choose a suitable dielectric substrate. There are numerous substrates that can be used for the design of microstrip patch antennas and

their dielectric constants are usually in the range of 2.2 $\leqslant \varepsilon_r \leqslant$ 12. Those desirable for antenna performance are substrates whose dielectric constant is in the lower end of the range to assure good efficiency, large bandwidth, and loosely bound fields for radiation into space (but at the expense of larger element size) [14]. Microstrip patch antennas radiate primarily because of the fringing fields between the patch edge and the ground plane. The radiation increases with frequency, thicker substrates, lower permittivity, and originates mostly at discontinuities [14].

This work was designed based on a commercial substrate from Rogers namely, the RO3003, with ½ Oz electro-deposited copper on each side, and total thickness of 0.5mm including the copper sheets [58]. RO3003 offers a relatively stable dielectric constant of 3.0±0.04 at 10GHz and low dissipation factor of loss tangent 0.001. Its dielectric constant versus temperature is displayed in Figure 10 and over frequency in Figure 11 [58], retaining the value of 3 for the relative dielectric constant, ε_r.
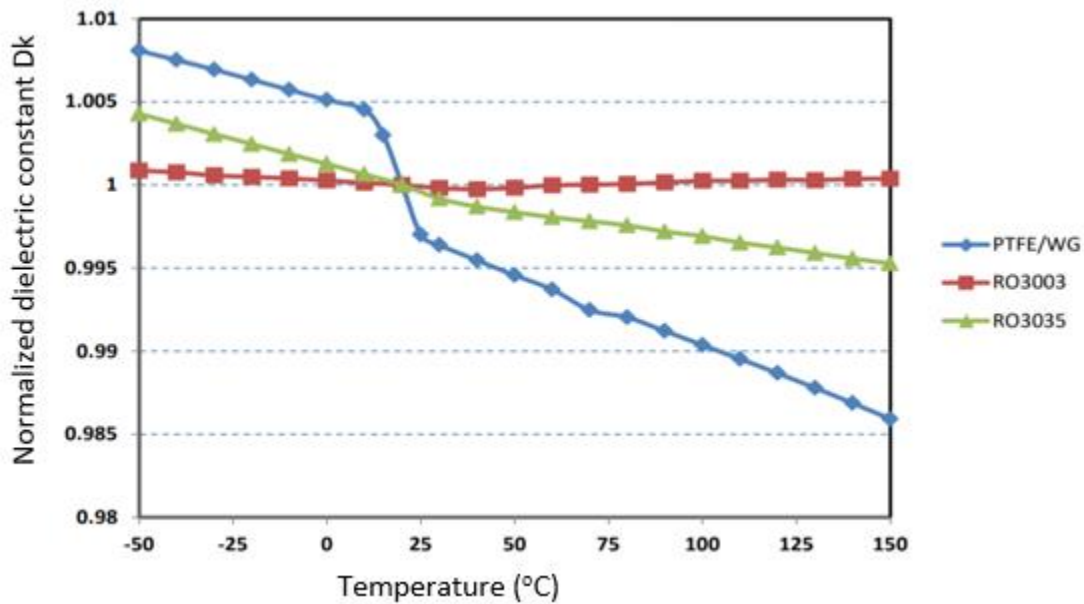

Figure 10 RO3000 series normalized dielectric constant over temperature [58]
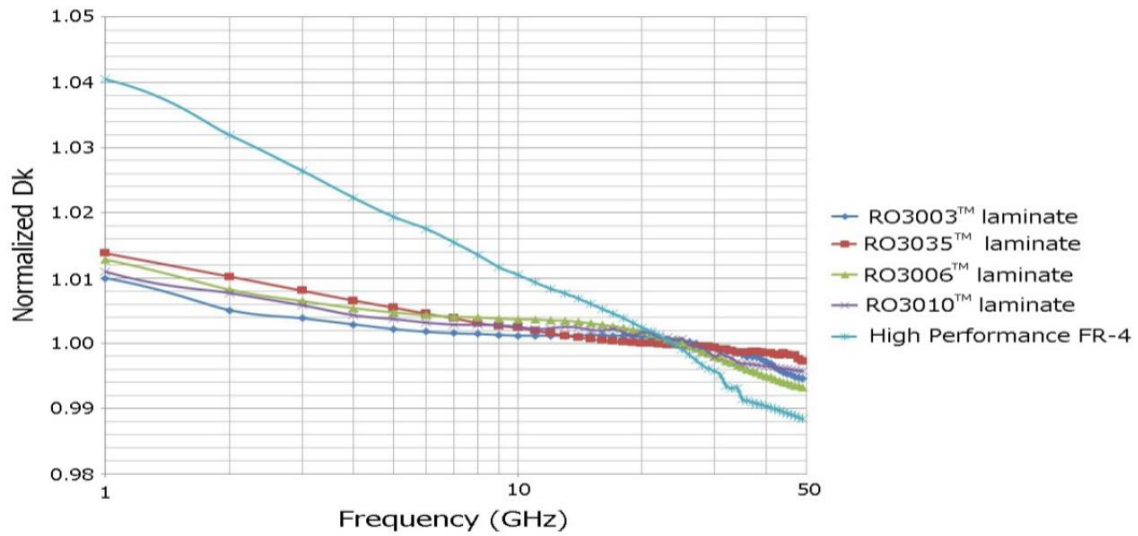
Figure 11 RO3000 stability of dielectric constant over frequency [58]

Five different values of thickness are available in the datasheet of the RO3003 Substrate. So we simulated a circular patch antenna of diameter of 3.2mm to see the effect of the substrate thickness on the antenna resonating frequencies and impedance bandwidth. From Figure 12, we can note that thinner thickness will perform a higher resonate frequency but will result in a narrower impedance bandwidth. To keep fulfill size limitation requirement in mobile applications, 0.5mm substrate thickness was retained in this design.
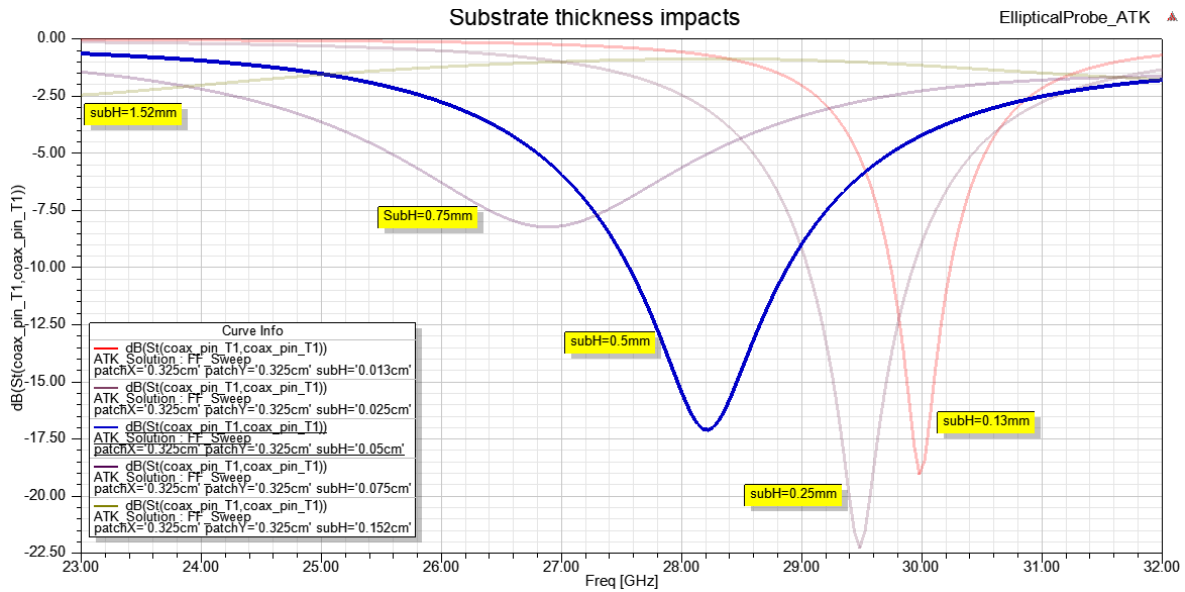
Figure 12 Substrate thickness impacts on resonate frequency

3.3 Patch Antenna Feeding Techniques

Various feeding technologies are available such as microstrip lines edge feed, slot apertures, probe feed, aperture coupling or proximity coupling [14].

3.3.1 Probe feed

As shown in Figure 13, probe feed via coax cable is achieved by connecting the inner conductor of the cable to the radiation patch antenna while its outer conductor is attached to the ground plane [1]. Coaxial feeding is easy to implement, has low spurious radiation, and easy to match while its disadvantages are its narrow bandwidth and the difficulty to model since the feeding pin will bring extra parasitic inductance, which need to be accurately calculated and modeled while the inductance will vary based on the substrate thickness.
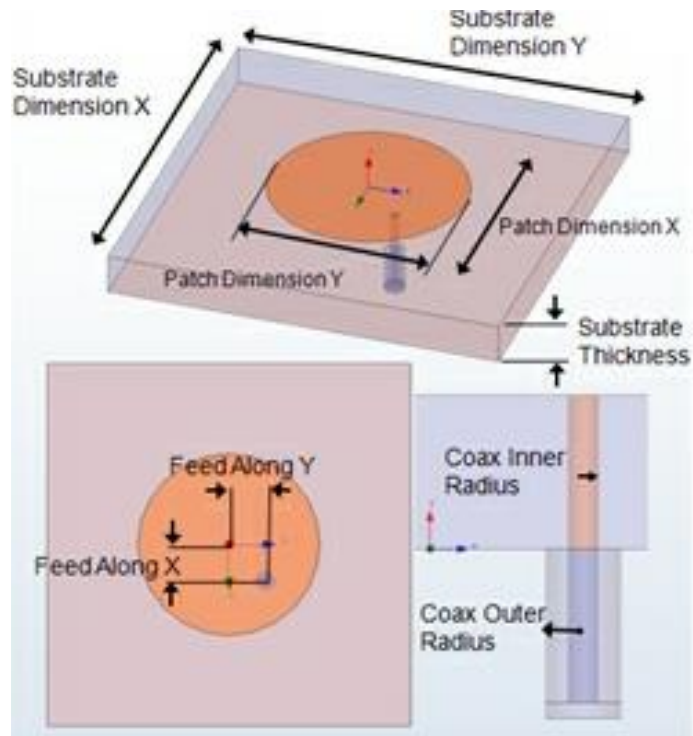
Figure 13 Probe feed in antenna design [66]

3.3.2 Microstrip feeds

Microstrip feed can be fabricated on the same plane of the patch antenna. It is easy to match by controlling the inset position, and easy to be modeled in the design simulations. It can be designed as inset feed, quart-wavelength transmission line feed and coupled indirect feed. However, the disadvantage of this method is that as substrate thickness increases, surface wave and spurious feed radiation increase, which limits the bandwidth.

Inset feed

The inset distance in Figure 14 can be used to adjust the feeding impedance matching with the antenna patch. Most circular patch inset feed designs need simulation optimization. The

equation below for rectangular patch inset can be taken as reference for a given operation frequency [62][63]

$$R_{in}(s) = R_{in\,Patch\,edge}\cos^2(\frac{\pi}{L}x_o) \qquad (3.1)$$

with *s* the inset length, $R_{in\,Patch\,edge}$ the edge antenna resistance, and *L* the rectangular patch length (side parallel with feed line).
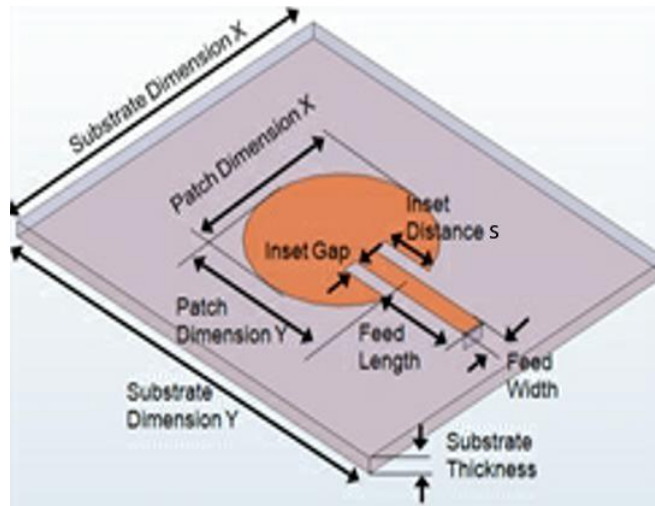

Figure 14 Inset feed in antenna design [66]

Quarter-Wavelength Transmission Line feed

Quarter wavelength feed has been used in this work because of its easy impedance control and suitability for higher frequency antenna design, as shown in Figure 15. Quarter wavelength transmission line of characteristic impedance Z_1 (Edge feed line) can be used to match the microstrip antenna Z_A to a transmission line of characteristic impedance Z_o as in (3.2),

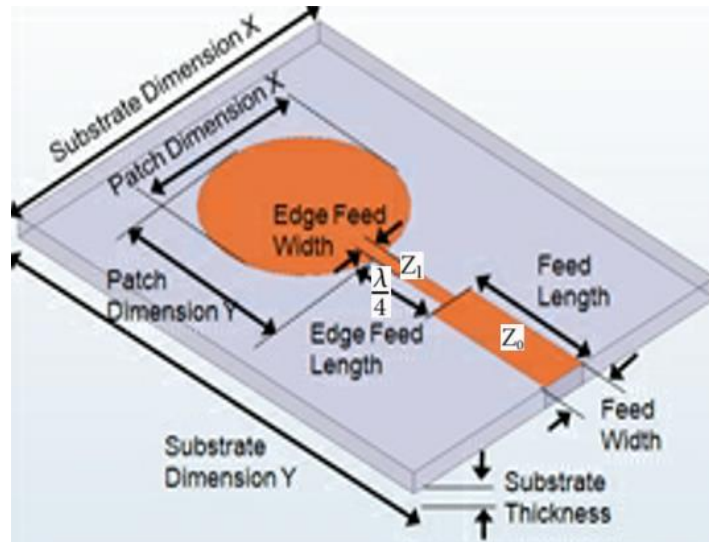$$Z_1 = \sqrt{Z_o Z_A} \qquad (3.2)$$

Figure 15 quarter-wavelength feed in antenna design [66]

3.3.3 Aperture coupling feed

The aperture coupling feed technology is a relatively recent non-contacting feeding technique. It consists of two substrates separated by a ground plane. On the bottom side of the lower substrate there is a microstrip feed line whose energy is coupled to the patch through a slot on the ground plane (Figure 16). This structure allows independent optimization of the feed mechanism and the radiating element substrate. A high dielectric material is used for the bottom substrate to tightly coupled fields to do not produce spurious radiation and a thick low dielectric constant for the top substrate to produce broadly wide fringing fields, yielding to a better radiation. The ground plane between the substrates also isolates the feed from the radiating element and minimizes interferences of spurious radiations for pattern and polarization purity. However, this feeding technique will increase the design overall thickness, which is not favorable for space limited mobile devices. It also increases difficulty in fabrication, which is not favorable for commercial mass production.
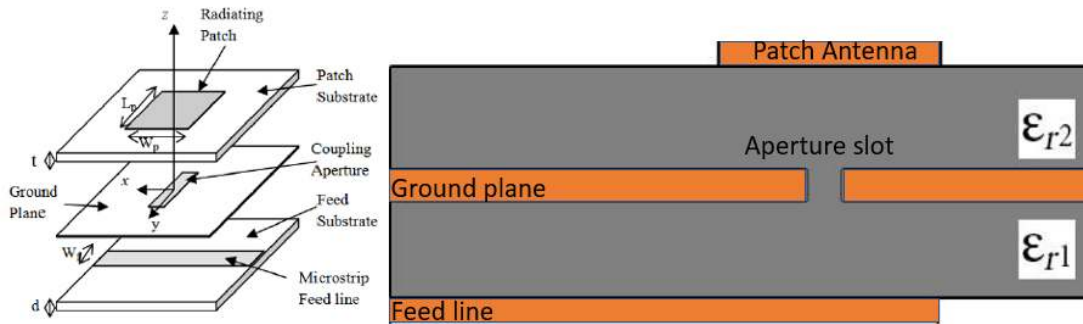
Figure 16 Aperture feed in antenna design [14].

3.3.4 Proximity coupling feed

Proximity coupling exhibits the larger bandwidth with low spurious radiation. Its coupling mechanism is capacitive by nature. Length of feeding stub and width to length ratio of patch are used to control matching. The major disadvantage of this technique is that it is difficult to fabricate due to the use of two dielectric layers that need proper alignment and also there is an increase in the antenna thickness, which is not favorable in mobile devices and manufacturing mass production [7]. The proximity coupling feed structure is shown in Figure 17.
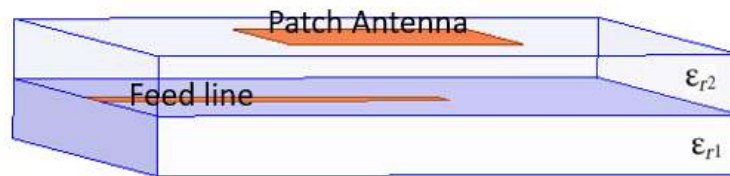

Figure 17 Proximity coupling feed in antenna design [14]

3.4 Patch antenna models

Various models can be used to predict the resonant frequency, bandwidth, input impedance and radiation characteristics of a microstrip patch.

3.4.1 Transmission line model

Transmission line model is simple to implement and offers good insight into the behaviour of the microstrip antenna; however, it is the least accurate of the methods [14].

When the transmission line is fabricated on a thin substrate, $\frac{w}{h} > 1$ (with h the height of the dielectric substrate and w the width of the patch), the effective permittivity ε_e can be expressed as in (3.3) ,

$$\varepsilon_e = \frac{\varepsilon_r + 1}{2} + \frac{\varepsilon_r - 1}{2}[1 + 12\frac{h}{W}]^{-1/2} \ , \qquad \frac{w}{h} > 1 \qquad (3.3)$$

As for the guided wavelength, it is given by

$$\lambda_g = \frac{\lambda_o}{\sqrt{\varepsilon_e}} \qquad\qquad (3.4)$$

with λ_o the wavelength of the free space. The corresponding characteristic impedance of the microstrip transmission line can be expressed as in (3.5), for $w/h \geqslant 1$

$$Z_o = \frac{120\pi}{\sqrt{\varepsilon_e}[\frac{W}{h} + 1.393 + 0.667ln\left(\frac{W}{h} + 1.444\right)]} \ , \qquad \frac{w}{h} \geq 1 \qquad\qquad (3.5)$$

while the resonance frequency of the rectangular microstrip patch antenna formula is given in (3.6) with L_e the effective length, and c is the light velocity in free space (assuming that $\varepsilon_r = 1$ due to the substrate is air)

$$f_0 = \frac{c}{2L_e\sqrt{\varepsilon_e}} \tag{3.6}$$

Theoretical resonance frequency of the rectangular microstrip patch antenna for the fundamental mode can be calculated using (3.7),

$$f_0 = \frac{c}{2L_e} \tag{3.7}$$

When a flat conducting strip of width w and thickness t, is placed on a grounded substrate material of height h and relative permittivity ε_r, the electric and magnetic fields in the vicinity of the conducting strip (Figure 8) are similar to the field distribution in a TEM mode and, are thus called quasi-TEM. Most of the fields are concentrated within the substrate, between the conducting strip and the ground plane; however, there are also fringing fields in the air region above the microstrip line. The width of the patch is related to the resonance frequency of the rectangular microstrip patch as,

$$W = \frac{c}{2f_o}\sqrt{\frac{2}{\varepsilon_r + 1}} \tag{3.8}$$

To design a microstrip patch for a given resonance frequency, substrate thickness, and permittivity, (3.8) can be first used to determine a suitable patch width.

In the transmission line model, the microstrip patch radiates from the fringing fields at either end of the patch length. This is similar to the radiation of two rectangular slots of length W and width ΔL separated by a distance L, as in Figure 18.

(a) Physical Patch

(b) Two-slot radiation model

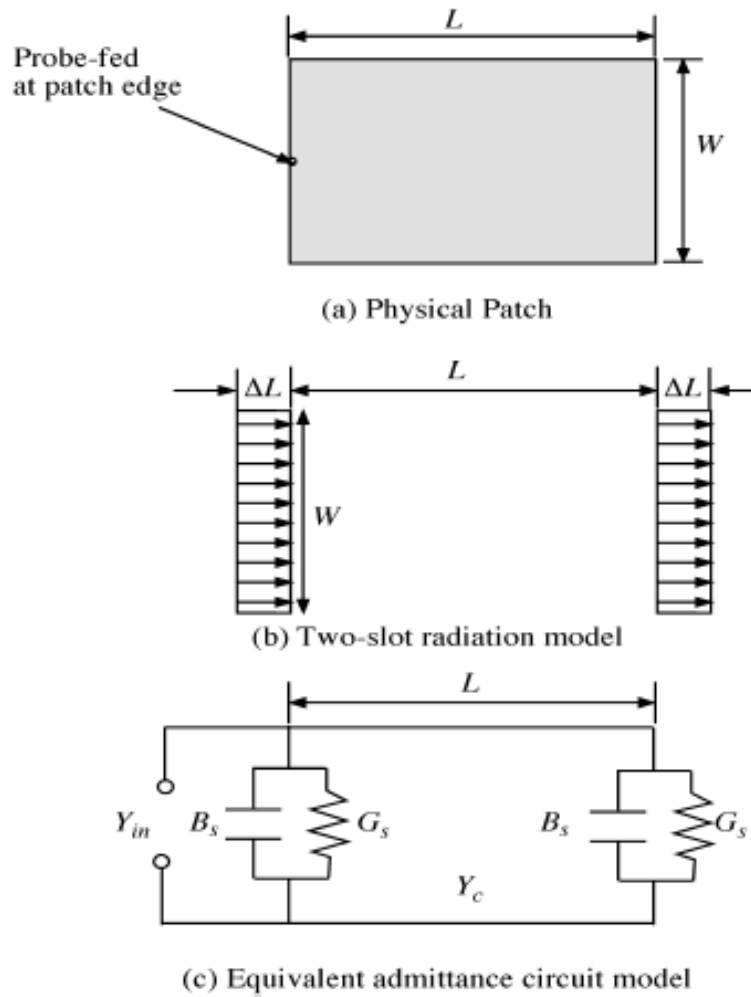(c) Equivalent admittance circuit model

Figure 18 Fringing Fields of the Microstrip Line [14]

Antenna is then modeled as a transmission line, with characteristic impedance Z_c or admittance Y_c, and length L. In this model, there are two slots on either side of the antenna, with an admittance Ys = Gs + jBs, as in Figure 18. The values for conductance (Gs) and slot susceptance (Bs) of a slot of width W with a uniform field distribution are given by (3.9) and (3.10), respectively:

$$G_s = \frac{W}{120\lambda_0}(1 - \frac{1}{24}(k_o h)^2) \qquad (3.9)$$

and

$$B_s = \frac{W}{120\lambda_o}(1 - 0.636(k_o h)) \qquad (3.10)$$

The transmission line will have extension of length 2*ΔL (i.e., at the both edges of the length directions), due to fringing effect, leading to

$$L_e = L + 2\Delta L \qquad (3.11)$$

The dimensions of the patch along its length can be then extended on each end by a distance ΔL, which is given empirically by Hammerstad as (3.12),

$$\Delta L = 0.412h \frac{(\varepsilon_{reff} + 1)(\frac{W}{h} + 0.264)}{(\varepsilon_{reff} - 0.258)(\frac{W}{h} + 0.8)} \qquad (3.12)$$

3.4.2 Cavity model

Cavity model is more complex compared to the transmission line model, but it will offer more accuracy and physical insight. The cavity is composed of two electric conductors at the top and the bottom to represent the patch and the ground plane and by a cylindrical perfect magnetic conductor around the circular periphery of the cavity. The dielectric material of the substrate is assumed to be truncated beyond the extent of the patch.

For a patch circular antenna designed on thin substrate of height h and assuming a radius $Cr \gg h$, the effective radius (considering fringe effects) can be expressed as (3.13),

$$c_{re} = c_r \left[1 + \frac{2h}{\pi \varepsilon_r c_r} \left(\ln\left(\frac{\pi c_r}{2h}\right) + 1.7726 \right) \right]^{1/2} \qquad (3.13)$$

3.5 Antenna Quality Factor

Antenna quality factor Q can be used to determine the impedance bandwidth (BW) of a microstrip antenna as function of the VSWR *s*, as in (3.14) [14]

$$BW = \frac{s-1}{Q\sqrt{s}} \qquad (3.14)$$

with

$$Q = \left(\frac{1}{Q_d} + \frac{1}{Q_c} + \frac{1}{Q_{sp}} + \frac{1}{Q_{sw}}\right)^{-1} \qquad (3.15)$$

i.e., the quality factor can be expressed as a sum of different quality factors in equations (3.16)-(3.21), with Q_d due to the dielectric losses (function of $\tan\delta$, the loss tangent of the substrate),

$$Q_d = \frac{1}{\tan\delta} \qquad (3.16)$$

Q_c the Q-factor due to the conductor losses,

$$Q_c = \frac{1}{2}\eta_o\frac{k_o h}{R_s} \qquad (3.17)$$

where *Rs* is the surface resistivity given by (3.18),

$$R_s = \sqrt{\frac{\pi f \mu_o}{\sigma}} \qquad (3.18)$$

with μ_o the free-space permeability ($4\pi \times 10^{-7}$ F/m) and σ the conductivity, and Q_{sp} the Q-factor due to the space wave component of the antenna radiation,

$$Q_{sp} = \frac{3}{16}\frac{\varepsilon_r}{pc_1}\frac{L_{eff}}{W_{reff}}\frac{\lambda_o}{h} \qquad (3.19)$$

where p should be calculated as (3.20),

$$p = 1 + \frac{a_1}{10}\left(k_o W_{reff}\right)^2 + \frac{3}{560}\left(a_1{}^2 + 2a_2\right)\left(k_o W_{reff}\right)^4$$
$$+ \frac{1}{5}a_3\left(k_o L_{reff}\right)^2 + \frac{1}{70}a_1 a_3\left(k_o W_{reff}\right)^2\left(k_o L_{reff}\right)^2 \tag{3.20}$$

with

$$a1 = -0.16605$$

$$a2 = 0.00761$$

$$a3 = -0.0914153$$

and $c_1 = 1 + \frac{-1}{\varepsilon_r} + \frac{2}{\varepsilon_r{}^2}$,

Q_{sw} is the Q-factor due to the surface wave component of the antenna radiation,

$$Q_{sw} = Q_{sp}\frac{e}{e-1} \tag{3.21}$$

where e, p_{sp} and p_{sw} are given by

$$e = \frac{p_{sp}}{p_{sp} + p_{sw}} \tag{3.22}$$

$$p_{sp} = \frac{1}{\lambda_o{}^2}(k_o h)^2(80\pi^2 c_1) \tag{3.23}$$

$$p_{sw} = \frac{1}{\lambda_o{}^2}(k_o h)^3\left(60\pi^3\left(1 - \frac{1}{\varepsilon_r}\right)^3\right) \tag{3.24}$$

3.6 Rectangular patch and circular patch antenna comparison

To compare the antenna performance between rectangular shape and circular shape, a rectangular antenna and a circular patch antenna were designed on RO3003 substrate at 28GHz. In this thesis, antenna simulations were performed on HFSS simulation tool from Ansoft [66], HFSS being one of the tools heavily used in industrial design environments [64].

Rectangular patch width W= 3.8mm was derived from Equation (3.8), while its length L=2.72mm was derived from equations (3.7), (3.11) and (3.12). As for the circular patch antenna, given the operating frequency of 28GHz, its radius can be calculated as [60],

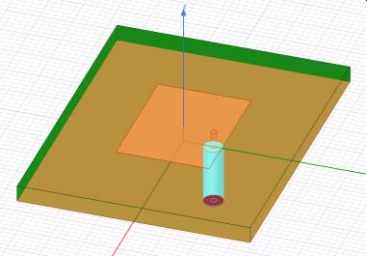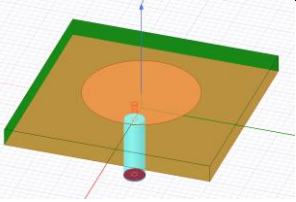$$F = \frac{8.791 \text{x } 10^9}{f_r \sqrt{\varepsilon_r}}$$

$$= \frac{8.791 \text{x } 10^9}{28 \text{x } 10^9 \sqrt{3.0}} = 0.1813 \qquad (3.25)$$

$$Cr = \frac{F}{\left[1 + \frac{2h}{\pi \varepsilon_r F} \left(\ln\left(\frac{\pi F}{2h}\right) + 1.7726\right)\right]^{1/2}} = 0.016 \ cm \qquad (3.26)$$

The comparison table (Table 4) leads to the similar conclusion as a comparison study reported in 2014 about a rectangular patch and a circular patch performance at X band [12], i.e., for the resonate frequency of 28GHz, both rectangular and circular patch antennas on the same RO3003 substrate have compactable dimensions, rectangular patch size as 3.8mmx2.72mm and circular patch diameter as 3.2mm. However, the circular patch antenna can perform on smaller substrate size as 4.5mmx4.5mm while the rectangular patch needs a substrate size of 9mmx7mm. From the board space point of view, circular patches are more suitable for space limited design such as mobile application.

Table 4 Rectangular patch vs. circular patch comparison

	Rectangular Patch	Circular Patch	Comments
Antenna Type			Both antennas were designed with probe feeding, resonate frequency at 28GHz.
Patch Dimension	Width=3.8mm (Equation(3.8)) Length=0.272mm(Equation (3.7), (3.11) (3.12))	Radius Cr=1.6mm (Equations (3.25), (3.26)	Both antennas have similar size
Substrate	RO3003, thickness 0.5mm Substrate width: 9mm Substrate Length: 7mm	RO3003, thickness 0.5mm Substrate width: 4.5mm Substrate Length: 4.5mm	Circular patch antenna can fit in smaller substrate dimensions
Impedance bandwidth	RL=-10dB impedance bandwidth as below, BW=f2-f1=28.3626-27.4747=0.8889GHz Center 27.9GHz, -15.14dB	RL=-10dB impedance bandwidth as below, BW=f2-f1=28.8285-27.1515=1.6970GHz Center 27.95GHz, -36.18dB	Circular Patch antenna perform a wider impedance bandwidth and a better S11 at resonate frequency

Gain	Rectangular patch peak gain as 7.6dB	Circular patch peak gain as 6.9dB	Rectangular patch have slightly advantage on gain and directivity
Radiation Pattern	Broadside radiation pattern, sidelobe level -11.5037dB	Broadside radiation pattern, sidelobe level -13.2868dB	Both rectangular and circular antenna radiated broadside, circular patch antenna has smaller sidelobe and backlobe,

ff_2D_GainTotal RectProbe_ATK

ff_2D_GainTotal EllipticalP
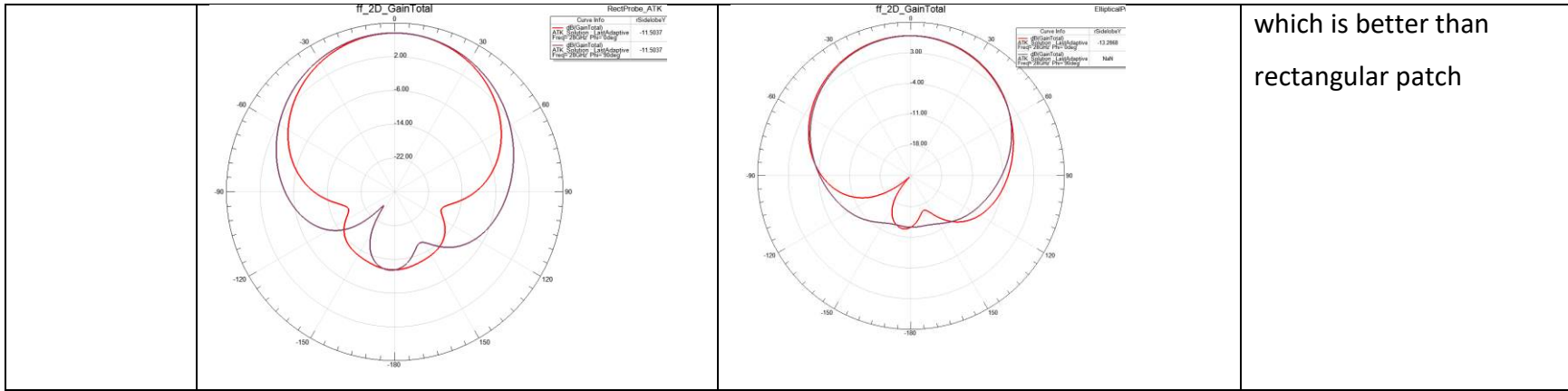
which is better than

rectangular patch

Also, the radiated performance comparison shows that the rectangular performs a slightly better in terms of gain, i.e., 7.6dB vs. 6.9dB for the circular patch. However, the circular patch shows a wider impedance bandwidth of 1.6970 GHz compared with the rectangular patch as 0.8889 GHz.

From the design specifications, as set in chapter 1, we need a small form factor to fit in mobile application chassis and wideband operating impedance bandwidth to hand shake among networks bands for upcoming 5G application. So, the form factor and impedance bandwidth weight more than gain. Thus, we selected the circular patch antenna as the radiation element.

3.7 Circular Patch Radiation Element Design

In this work, we then designed a circular patch radiation element on the Rogers RO3003 high frequency circuit substrate with relative dielectric constant of 3.0, loss tangent of 0.0013, and substrate thickness of 0.5mm with ½ Oz electro-deposited copper on each side. The optimized dimensions of the patch, depicted in Figure 19, are provided in Table 5 for 28GHz.
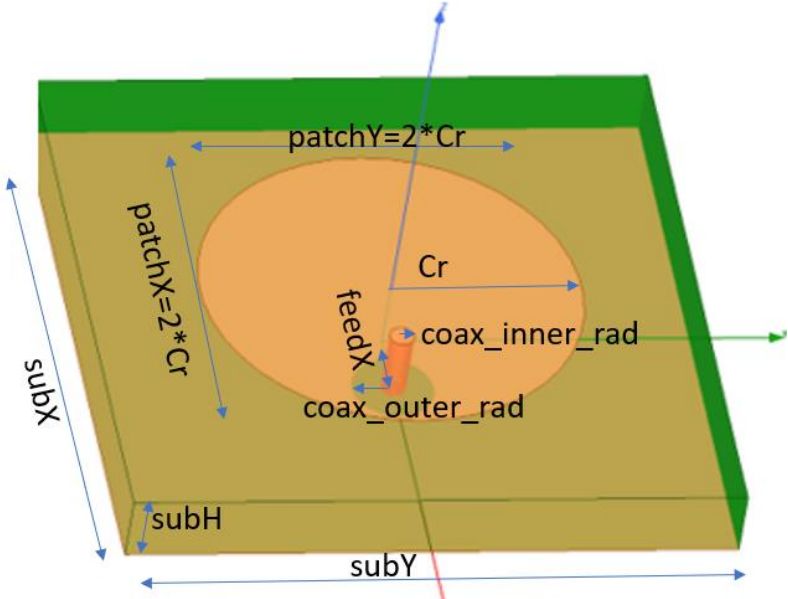

Figure 19 Circular patch antenna element

Table 5 Radiation circular element design parameters

Description	Variables	Value	Unit
Patch Radius	Cr	1.6	mm
Substrate X	subX	4.5	mm
Substrate Y	subY	4.5	mm
Substrate H	subH	0.5	mm
Feed X offset	feedX	0.5	mm
Feed Y offset	feedY	0	mm
Coax inner Radius	Coax_inner_rad	0.09	mm
Coax outer radius	Coax_outer_rad	0.3	mm

As shown in Figure 20, the simulated bandwidth is from 27.15 to 28.85 GHz (with a radiation pattern shown in Figure 21 and a peak gain of 6.9dB (Figure 22). The radiation pattern shows low back lobe radiation due to the full ground plane at the back. However, since the single radiation element can a gain of 6.9 dB, which is lower than design targets, an antenna array was considered and simulated to get higher antenna gain.

3.8 Linear antenna array with circular patch elements simulation

Different feeding techniques were discussed in Chapter 3.3 and the probe feeding was selected as initial design to avoid complicated structure design, friendly to manufacturing in mass production.

HFSS provides the DDM (Domain Decomposition Method) simulation method, which can simulate finite/infinite antenna array near field and far field performance with virtually adding boundary conditions on the radiation element unit.

First, a circular patch unit cell was built using the master/slave boundaries, to model a single element, as if it were in an infinite array environment, by enforcing field periodicity through master/slave boundary pairs. Also, it adds progressive phase shift between master and slave boundary to apply beam steering.

Then, the entire array was analyzed using the Finite Array DDM. DDM model accounts for edge affects, providing mutual coupling terms and allowing magnitude taper. It was then used to replicate the unit cell model in order to effectively solve full larger finite array mesh, as in Figure 23. The simulated antenna array started with four elements and a virtual array size of 4.5x18x0.5 mm^3; the feeding network not included in the simulation yet, will add extra size to the design.
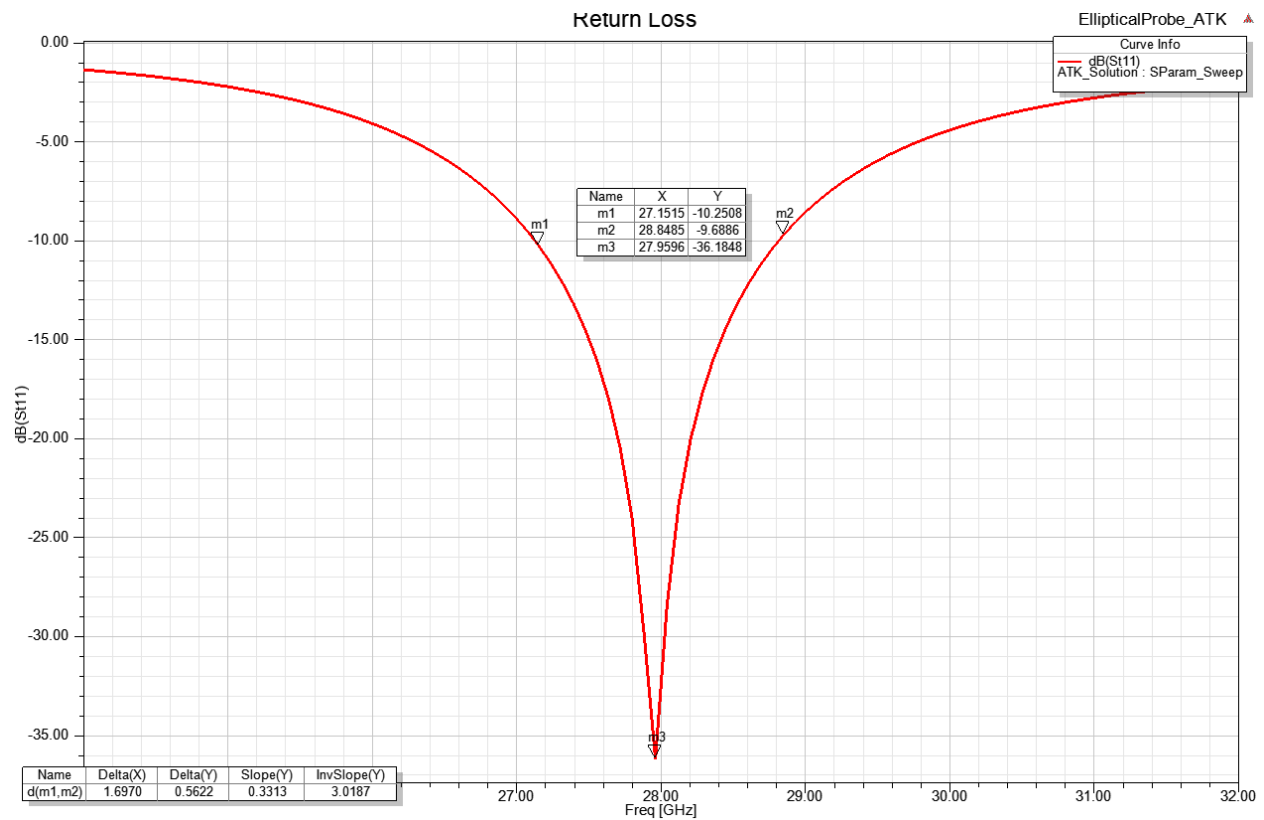

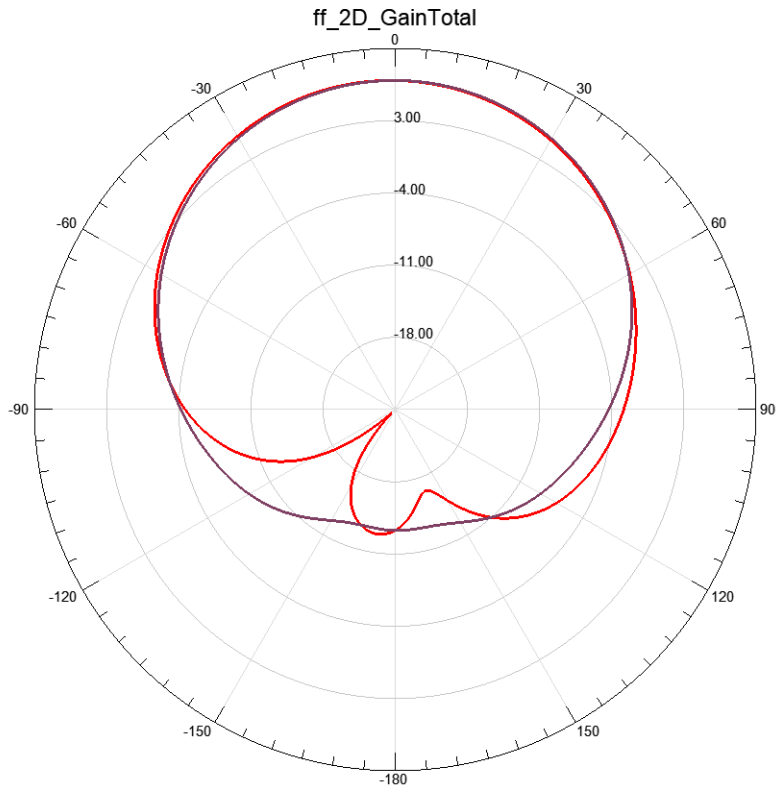Figure 20 Circular patch impedance bandwidth

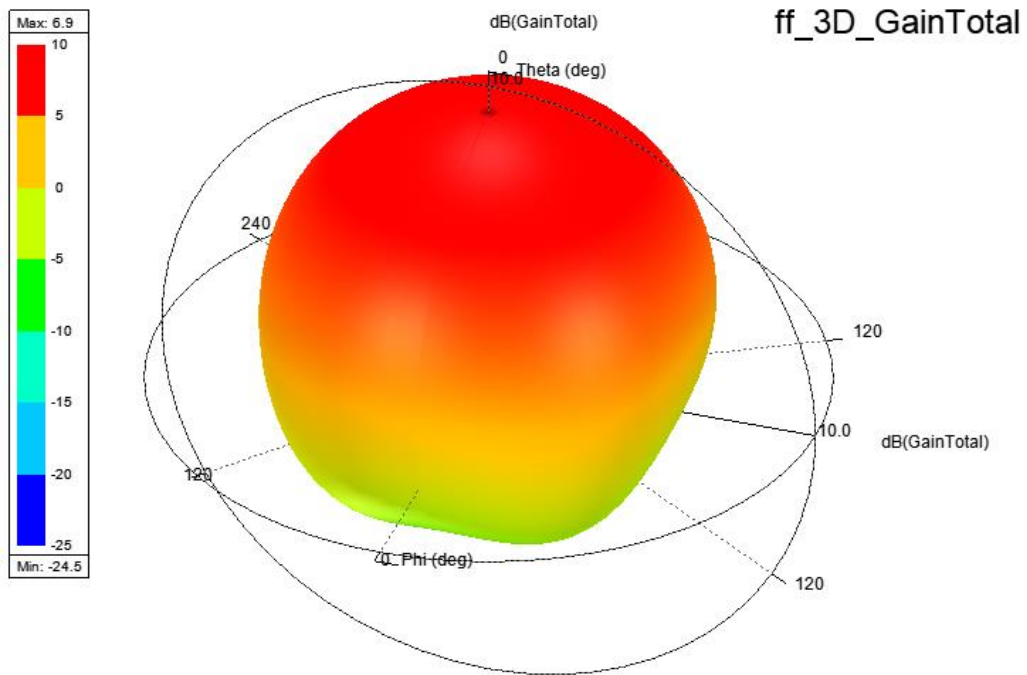Figure 21 Circular patch radiation pattern

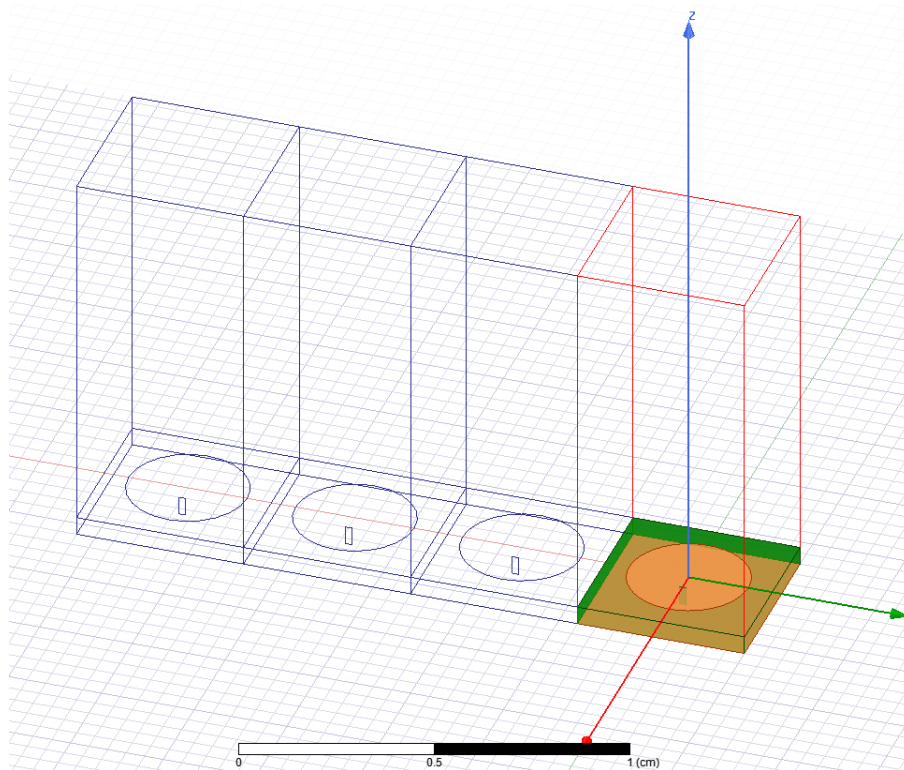Figure 22 Circular patch 3D gain plot

Figure 23 HFSS DDM simulation on circular array

The 3D radiation pattern plots are shown in Figure 24 while the 2D plots are displayed in Figure 25. From Figure 24, we can observe a narrow beam width of far field performance and broadside radiation. High side lobes can be observed in the plot but they can be further tuned and optimized during the feeding network design.

Figure 25 provides information of radiation pattern for the antenna array in Figure 23. Main beam from simulation is squint 30 degree clockwise. From these results, we can see that the gain achieved is 8.9dB, which is below the targeted value. Besides, the operating bandwidth is narrow. So we need to add more radiation elements in the linear array to widen operation bandwidth which will lead to bigger size. Also, the feeding network should be added and tuned.
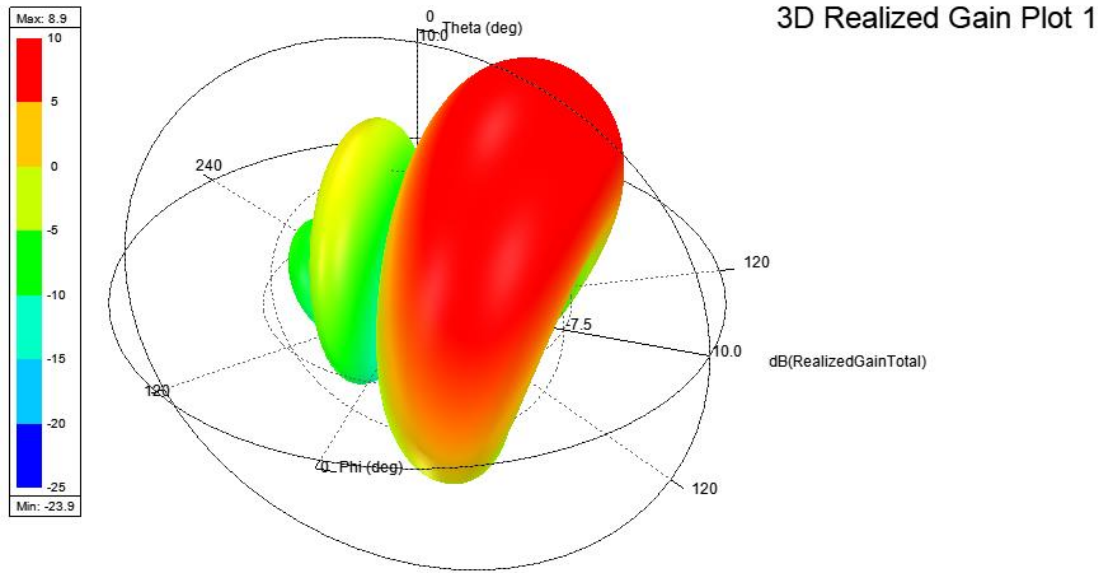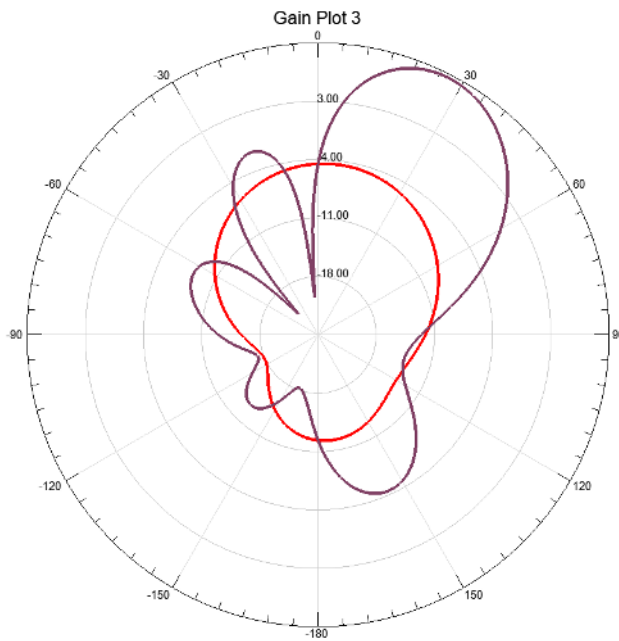
Figure 24 Circular array 3D gain plot

Figure 25 Circular array 2D radiation pattern

3.9 Conclusion

This chapter included the patch antenna parameter theoretical equations as well as a comparative study between a rectangular patch, taken as reference, and a circular patch, highlighting this latter as the most suitable for this work.

The linear antenna array with circular patch elements proposed and simulated in this chapter can achieve a gain of 8.9dB, i.e., lower than design target. Also, the operating band width is narrow and the feeding network needs to be designed. However, the feeding network will physically increase the overall size of the antenna design.

To solve the gain and impedance bandwidth issues without increasing size, the collinear Franklin design will be introduced in this design, as it will be detailed in the following chapter.

Chapter 4. Collinear Microstrip Array with Circular Patches

4.1 Franklin array with Circular patches

4.1.1 Why Franklin array

Franklin array key advantages are its high gain and broad impedance bandwidth, whereas the simplicity of the single feeding point in the antenna design structure. Franklin array original idea came from Franklin in 1924 [10]. It was a CoA from a long wire that had λ/4 U-shaped sections to provide phase shift to maintain in-phase feeding of straight λ/2 parts of the wire (Figure 2).

In principle, the standing wave current distribution on long straight wire produces n radiation lobes of the same level, depending on the number n of half-wave antenna sections. So, Franklin introduced non-radiating quarter-wave stubs to convert the original out-phase current distribution into an in-phased distribution of currents on collinear segments, thus producing only one major radiation beam.

This project targeted to design an antenna array suitable for the future 5G mobile devices. It should fulfill requirements of small form factor, conformal to various chassis structure, simple feeding requirement, relative high gain and broadband impedance bandwidth which can shake hands when hopping from network to another. The design started with the regular circular array.

4.1.2 Design dimensions

In this study, a collinear microstrip antenna array using a series feed network was designed at 28GHz with coplanar Franklin array as radiation elements, as shown in Figure 26. The design parameters listed in Figure 26 are specified in Table 6
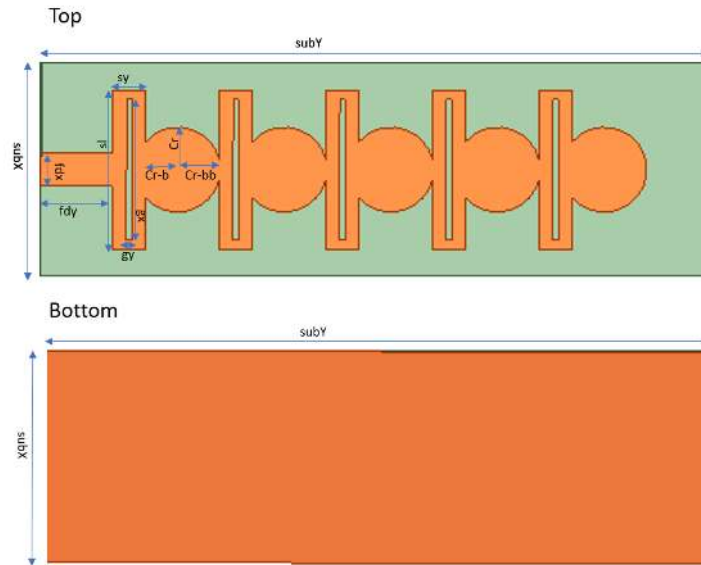
Figure 26 Circular Franklin antenna array

Table 6 Array design parameters

Description	Variables	Value	Unit
Patch Radius	Cr	1.6	mm
Substrate X	subX	8	mm
Substrate Y	subY	25	mm
Substrate H	subH	0.5	mm
Feed X	fdx	0.5	mm
Feed Y	fdy	2.68	mm
Phasing stub length	sl	6	mm
Phasing stub width	sy	1.26	mm
Gap length	gx	5.3	mm
Gap width	gy	0.2	mm
Patch left offset	b	0.4	mm
Patch right offset	bb	0.05	mm

4.2 Simulation results

4.2.1 Operation bandwidth

By introducing the phasing stub, The S_{11} plot of Figure 27 shows that the design target of bandwidth of 24.5–30.3 GHz has been achieved, with lower edge at 23.6GHz and higher edge at 30.2 GHz, i.e., a wide bandwidth of 24.54%.
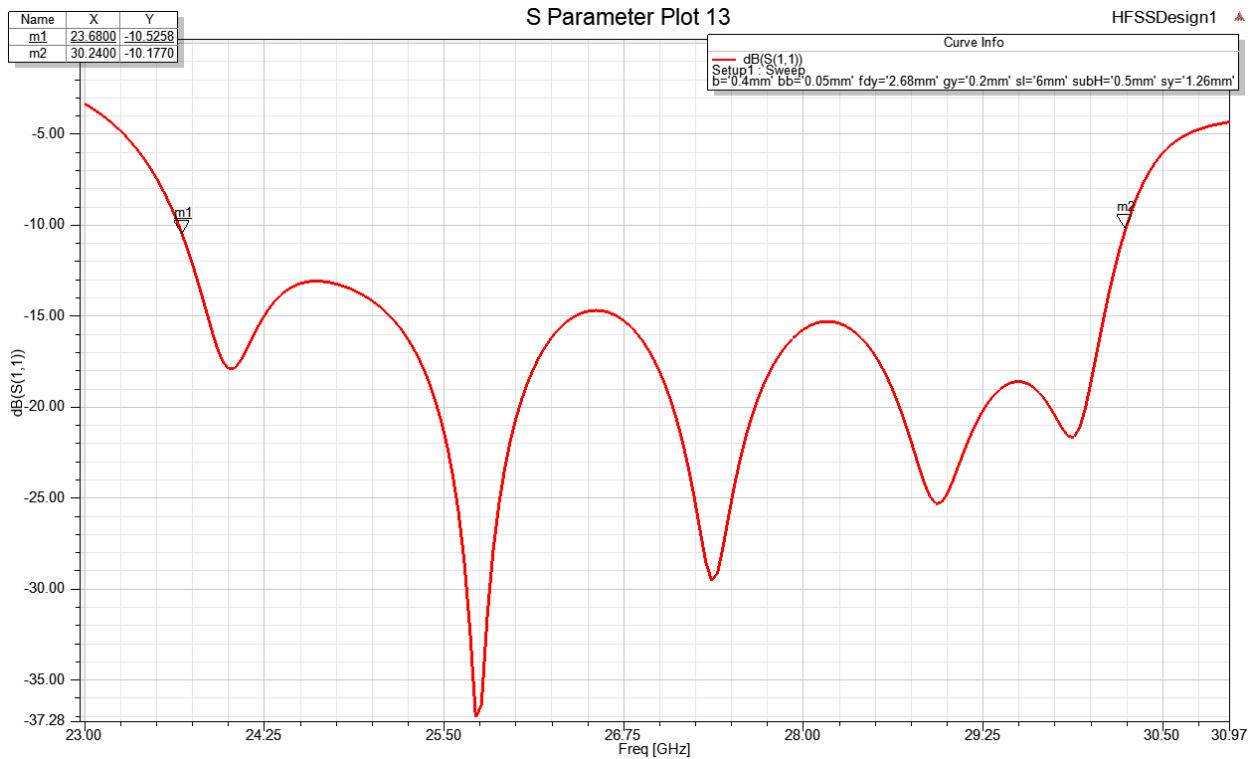

Figure 27 HFSS simulated Impedance bandwidth

4.2.2 Gain

The designed antenna gain plots at various frequencies in Figure 28 shows a peak value of 10.8dB.

24 GHz Gain
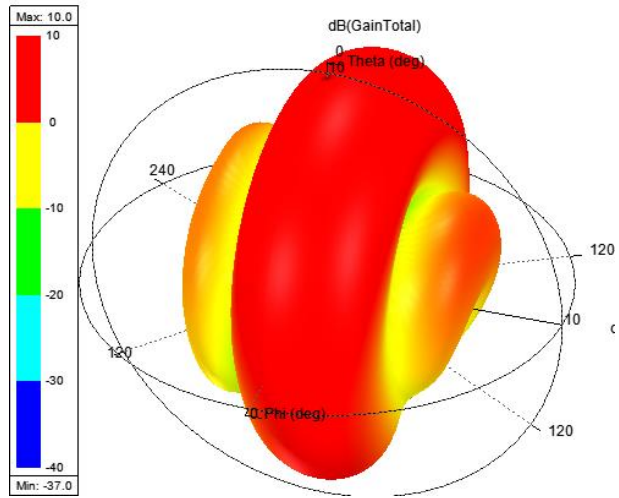
25 GHz Gain

26 GHz Gain

27 GHz Gain
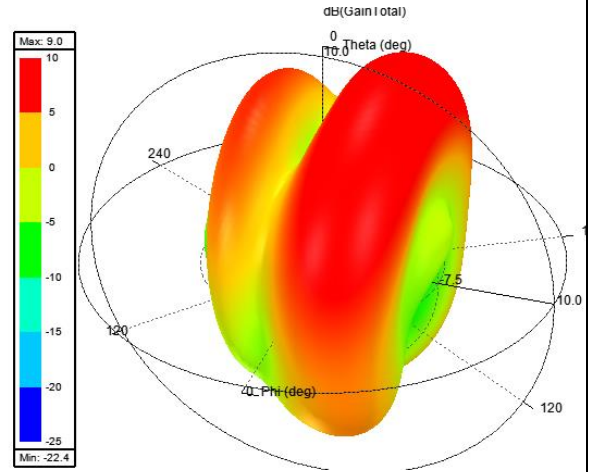
28 GHz Gain	29 GHz Gain
30 GHz Gain	

Figure 28 Gain 3D Polar Plots at various frequencies

The main beam steered from broadside to endfire direction performed similarly as the LWA antenna as reported in [11][26][28], and thus can be declared as a beam steering feature for the design [26][28] when scanning across frequencies like in LWA.

Note that when the antenna design covers broad band frequency, we need to adjust the phase shifter due to the wavelength change, i.e., it means that in order to keep a broadside beam for all frequencies, we need to introduce an ad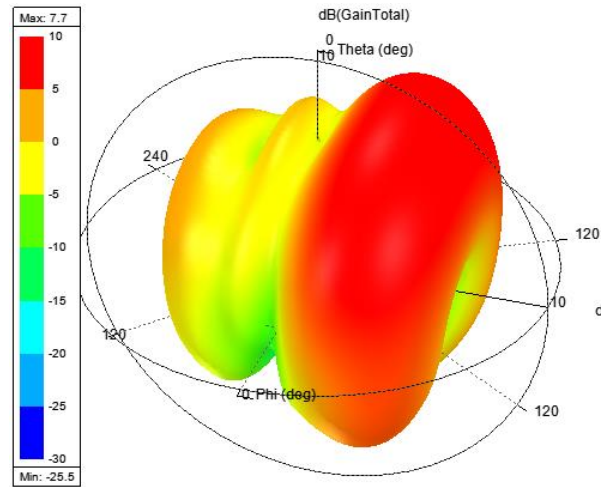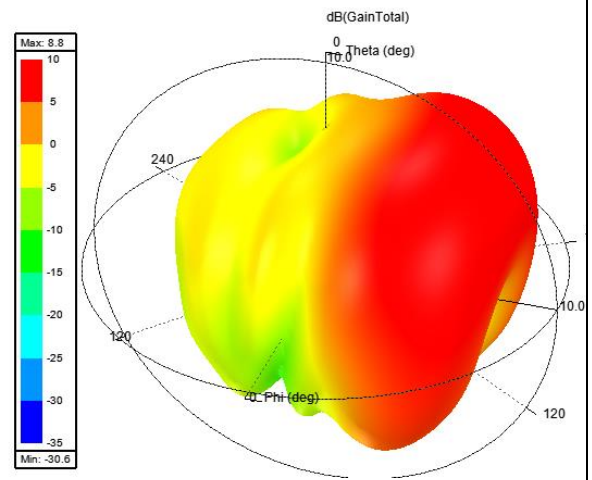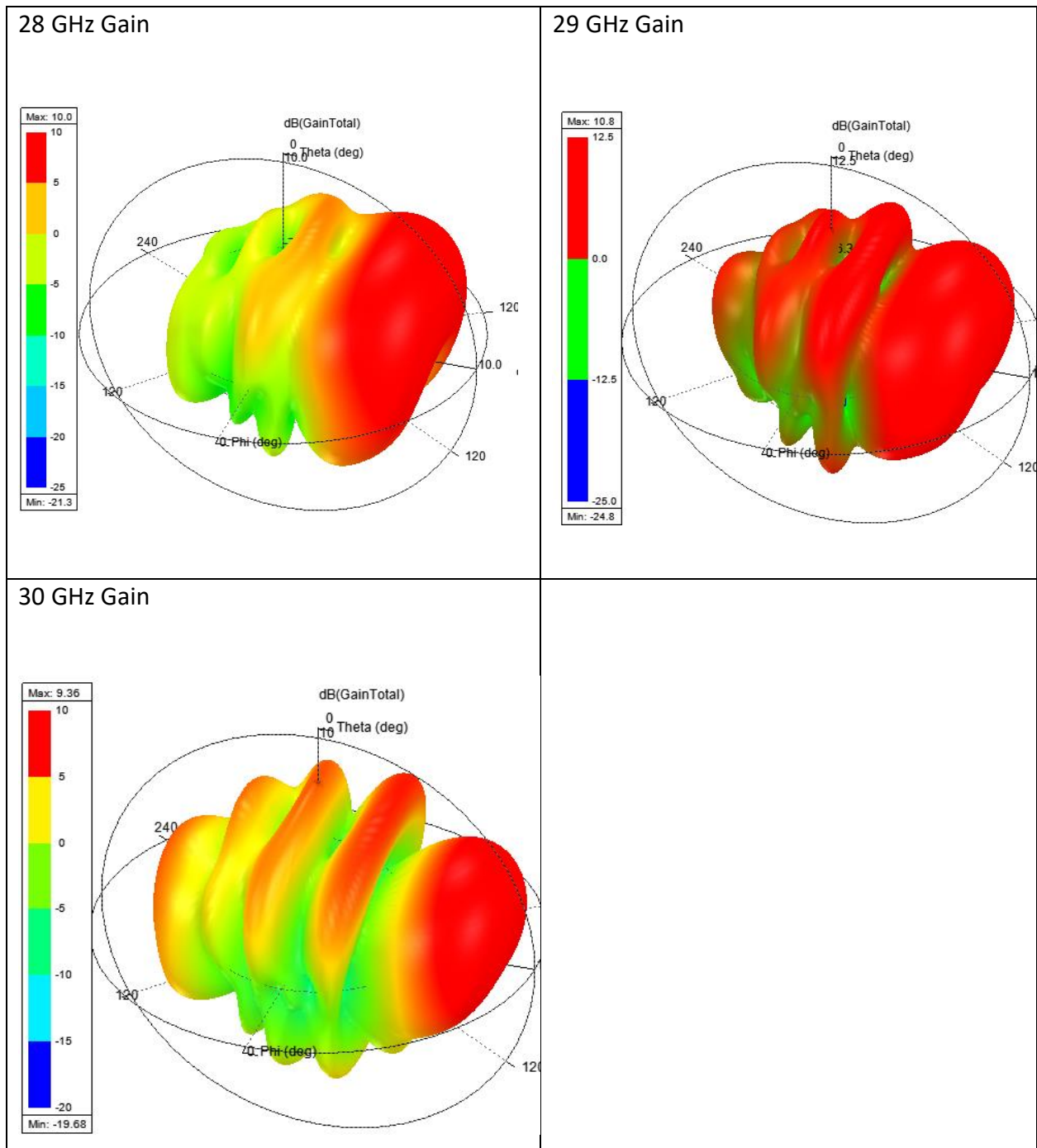justable phase shifter to compensate wavelength variations. In that case, introducing extra phase shifters will increase the feeding network dimensions, matching techniques, design cost and antenna losses. The Franklin array antenna works as low cost small form factor solution for the mobile application, which has to bear the beam squint impacts [11][26][28].

4.2.3 Gain variation over frequency

The designed antenna can achieve 10dB gain at 28 GHz and 10.8 dB gain at 29 GHz as shown in Figure 29.
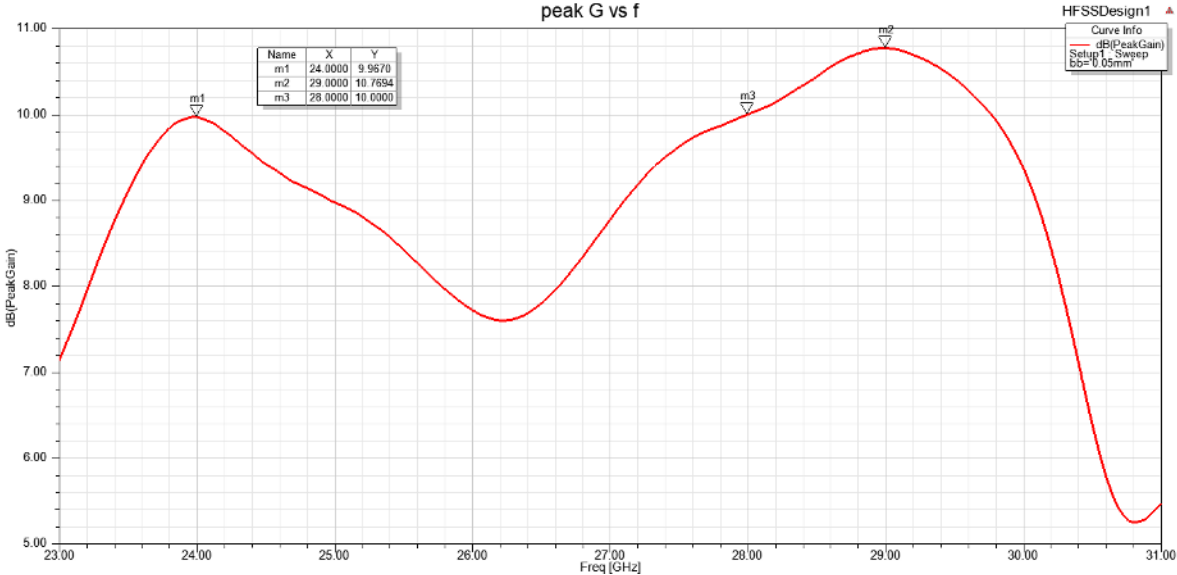
Figure 29 Peak gain variation across operation bandwidth

Figure 29 shows that when sweeping frequency from 23GHz to 31GHz, we can get a peak gain value of 10dB at 24GHz, 28GHz-29.8GHz, but the gain dipped below 9dB from 25 to 27 GHz. Such

gain variations across a broadband frequency range is in the nature of a collinear feeding structure with fixed phased shifter as reported in [26], which also shows a gain drop below 8dB from 25 to 27GHz.

4.2.4 Radiation efficiency over frequency

The designed antenna can achieve high efficiency over the whole operating frequency range, as Figure 30 shows. In this figure, the radiation efficiency includes the material dielectric loss from antenna material of copper and substrate. However, the reflection loss related with the mismatch in actual antenna matching circuit, is not included. Mismatch and reflection can be tuned in project implementation to leverage various performance trade-offs.
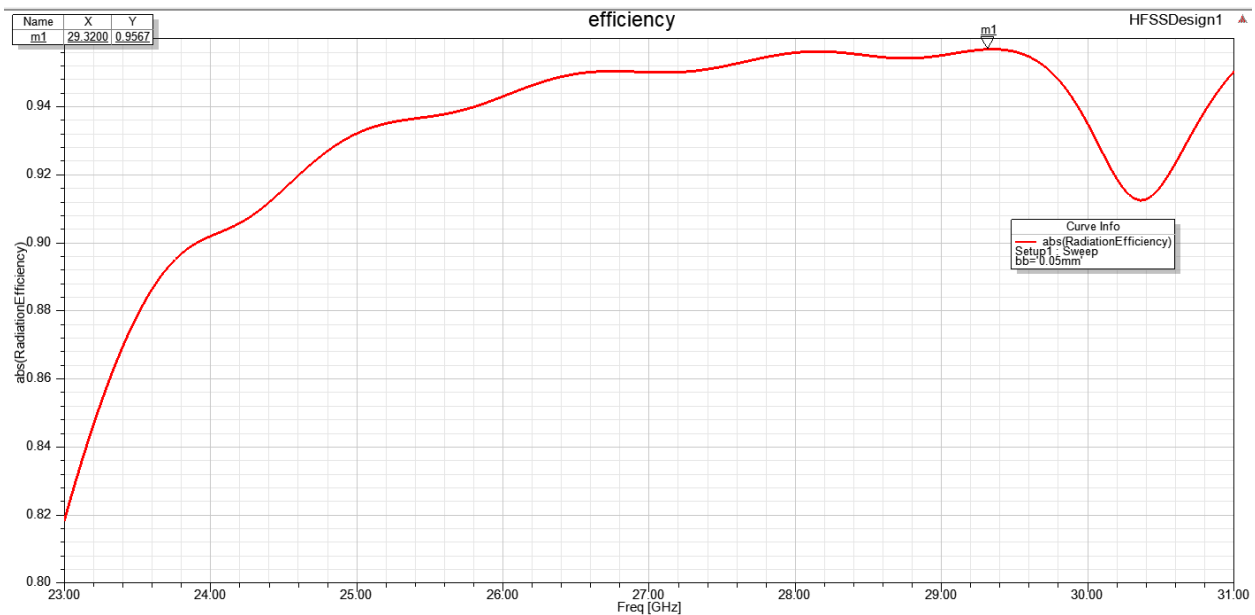
Figure 30 Radiation efficiency across operation bandwidth

4.2.5 Design optimization

Figure 32, Figure 33, and Figure 34 show the antenna design optimization to broad the operation bandwidth by controlling different patch cuts, phasing stub slot width, phasing stub width and phasing stub length, respectively.

Effects of patch left back off cut-b

Patch left cut can shift the operating bandwidth at lower frequency corner as in Figure 31. So the highlighted 0.4 mm cutoff was adopted in this design.
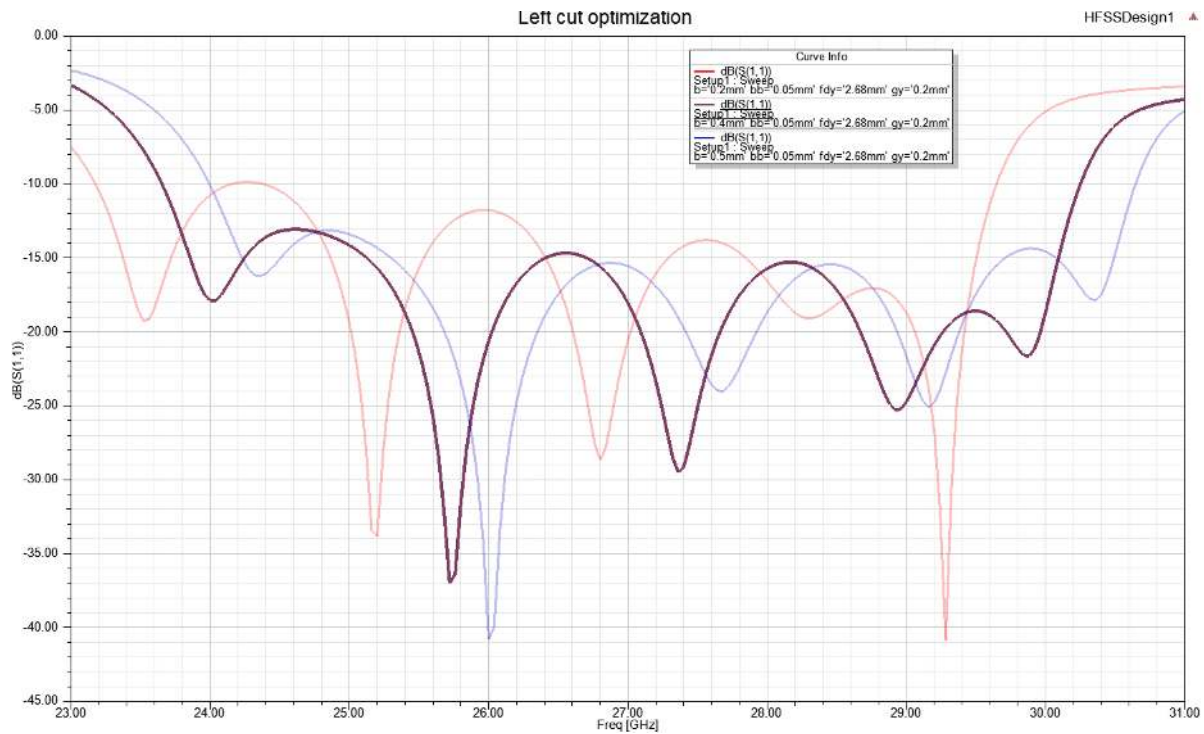
Figure 31 Effect of Circular left cut to control impedance bandwidth

From that figure we can also see that the larger circular patch left cut will shift the operating band towards the high frequency end. We therefore included the 0.4mm cut to control the circular patch size close to a half wavelength while keeping the impedance bandwidth from 23.6GHz- 30.3GHz, which meet the design specifications.

Effects of patch Phasing Stub slot-gy

Phasing stub slot can control the operating bandwidth lower frequency corner as in Figure 32, the highlighted 0.2mm slot width was adopted in this design. In fact, the phasing stub slot will control the phasing stub impedance, as Solbach reported in [11]. When sweeping the slot width from 0.1 to 0.5mm, we can see that the lower resonating frequency will shift toward higher frequencies. Our design selected 0.2 mm to keep the lower resonating edge at 23.6 GHz.
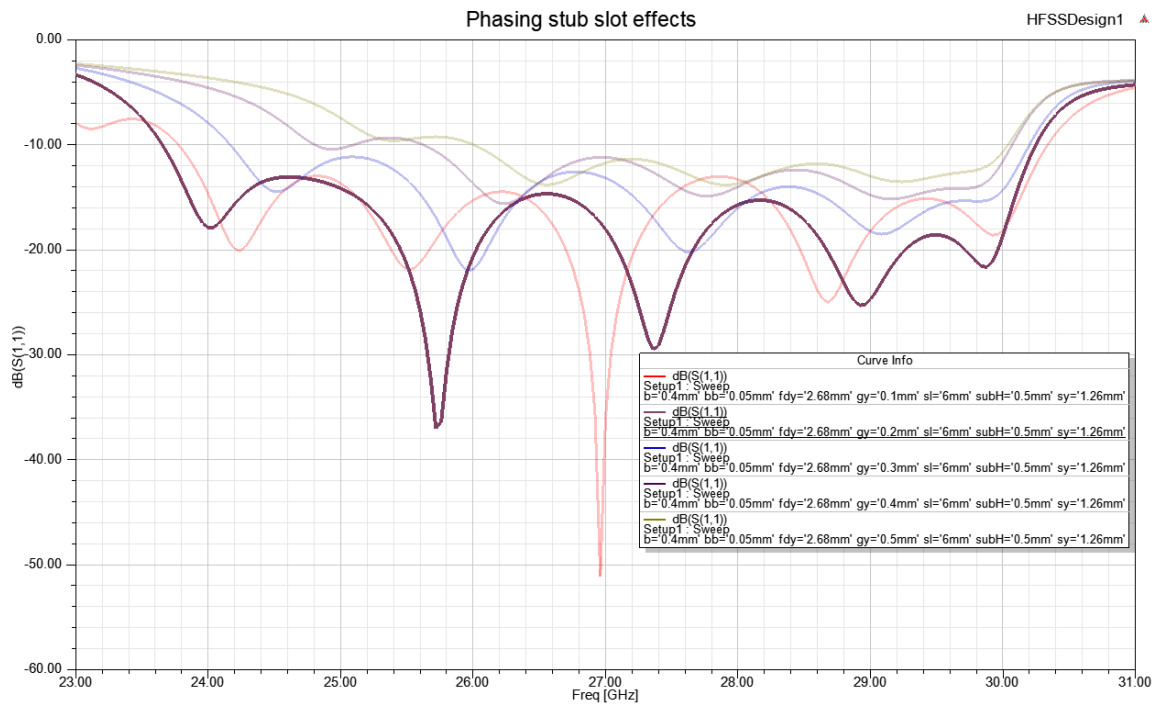
Figure 32 Effect of phasing stub slot width to control impedance bandwidth

Effects of Phasing stub width- sy

Phasing stub width effect on the design is not significant as in Figure 33, the highlighted 1.26mm stub width was adopted in this design.
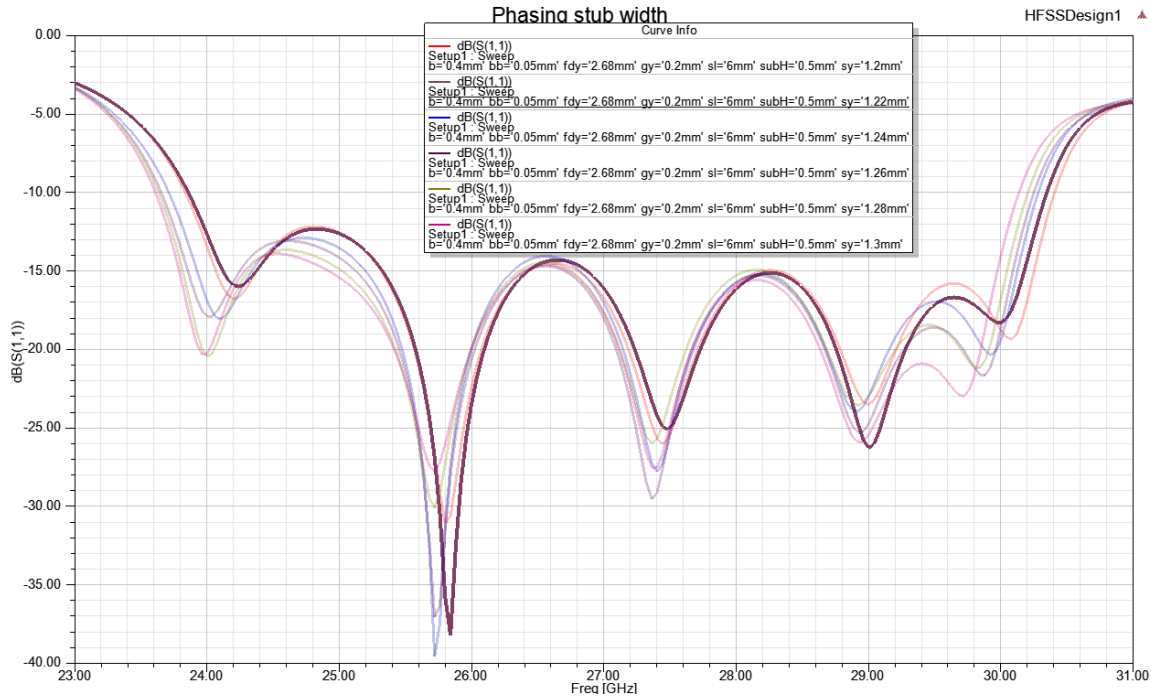
Figure 33 Effect of phasing stub width to control impedance bandwidth

Effects of Phasing stub length- sl

Phasing stub length can control the operating bandwidth higher frequency corner as in Figure 34, the highlighted 6 mm stub length was adopted in this design. This figure gives us the idea how the phasing stub length can shift the operating band. From the simulation we can observe that, when increasing the phasing stub length from 5.6 to 6.2mm, the operating band will shift toward the lower frequency direction. Our design selected 6mm to keep the phasing stub above the circular patch as well as half of the phasing stub width close to the quarter of lower frequency wavelength.

After above optimization rounds, the proposed antenna can be further improved to achieve wide operation bandwidth from 24.5-30.3GHz to 23.6–30.3 GHz with a peak gain staying at 10.8dB.
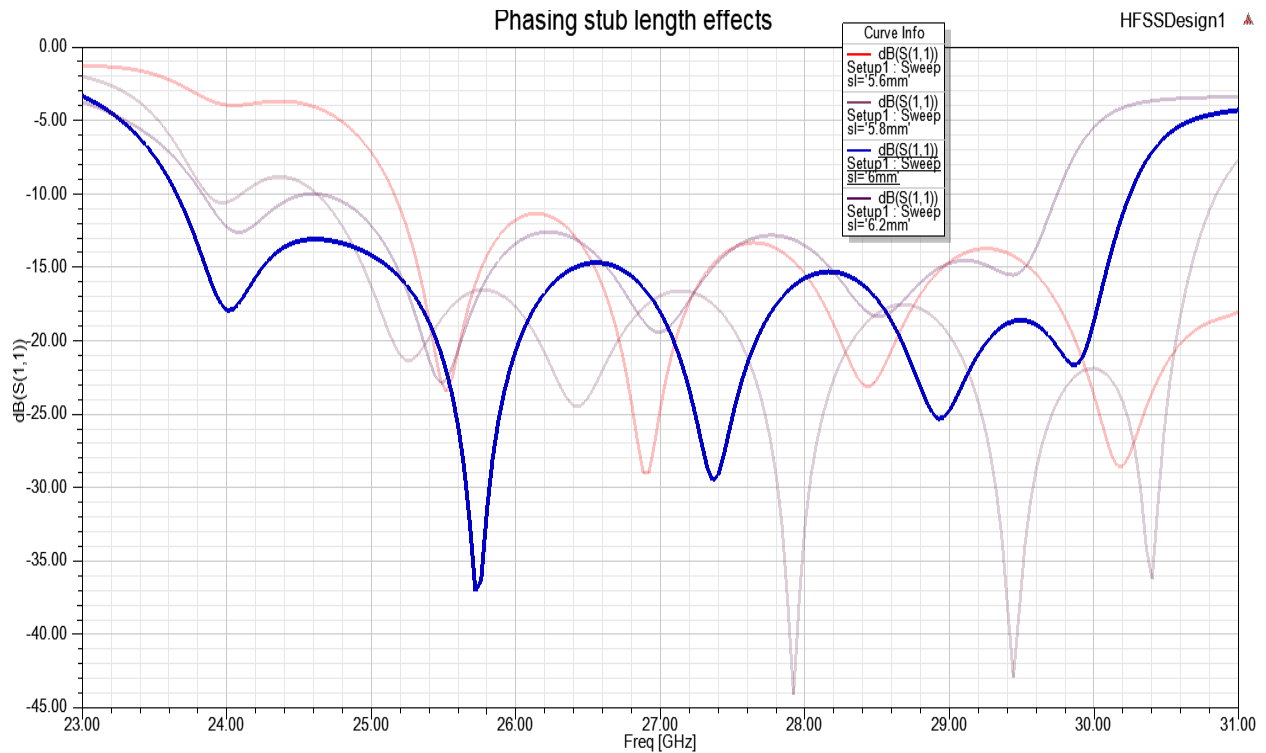
Figure 34 Effect of Phasing stub length to control impedance bandwidth

4.3 Conclusion

A circular patch was introduced in Franklin array in this chapter. The proposed antenna array with five circular radiation elements was able to achieve wide impedance bandwidth of 23.6-30.3 GHz, and peak gain of 10.8dB, which fulfill the original design targets.

This chapter also presented the radiation efficiency of the antenna array and gain variation across the whole frequency range. An optimization of antenna parameters was also performed to achieve better performance. The designed antenna has a small form factor of 8x25x0.5mm^3, low profile which is conformal with various mobile device chassis. Simulated gain and bandwidth fulfill the original design targets.

Chapter 5. Antenna Fabrication and measurements

5.1 Antenna Fabrication

The HFSS antenna design .dxf file was converted to a grb Gerber file for fabrication. Three collinear antenna arrays were fabricated on Rogers RO3003 substrate (Figure 35). Overall Antenna size is 8x25x0.5 mm^3 to fit in mobile limited space (Figure 36).
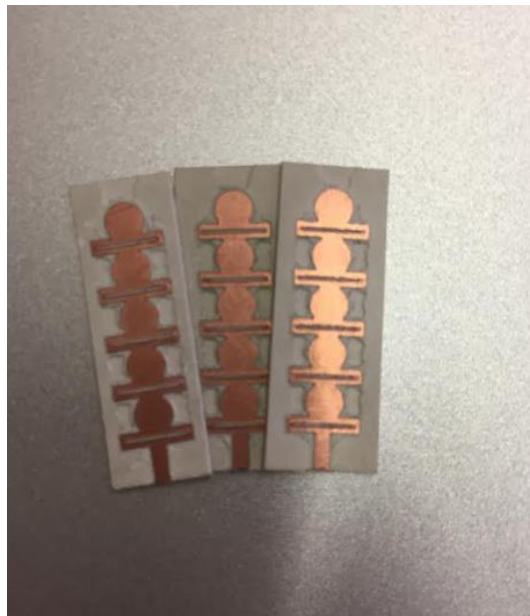
Figure 35 Fabricated Antenna arrays

Figure 36 Antenna size compared with a nickel

5.2 Antenna Lab measurements

5.2.1 Universal test fixture Anritsu 3680V

The antenna was fabricated and measured using the universal test fixture Anritsu 3680V (Figure 37). As specified on the Anritsu 3680V datasheet, the fixture consists of a fixed connector and a movable connector that can be positioned for substrates up to 50.08 mm (2 in) long. No center section is required. The substrate is held in place between spring loaded jaws. This allows the fixture to accommodate different devices without requiring a custom center section for each different length. Dielectric rods behind the jaws accurately position the substrate away from the launch to reduce fringing capacitance and contribute to the fixture's excellent repeatability.

Figure 37 Antenna measured with Anritsu 3680V test fixture

To de-embedded the Anritsu universal test fixture effects on the DUT, calibration has been performed before antenna test. Calibration of a VNA connected to a UTF can be performed directly in microstrip. The kit 36804B-10M can calibrate from 0.04GHz to 50 GHz. According to the test fixture calibration procedures in [68], two calibration modes were performed including

Open-Short-Load (OSL) and Line-Reflect-Line (LRL). OSL calibrations are the basic calibration but least accurate, especially for large reflections. LRL was performed also to cover a certain operating frequency range and lower frequencies. This calibrates out the mismatch that results from the transition between coax to microstrip.

5.2.2 R&S ZVA67 network analyzer

S_{11} parameter was measured on the R&S ZVA67 network analyzer, Figure 38. R&S ZVA67 supported measurement frequency from 10MHz up to 67 GHz, with a dynamic range shown in Figure 39 [69].

Note that all three fabricated antennas gave almost identical results. So we will display only the results of one antenna.
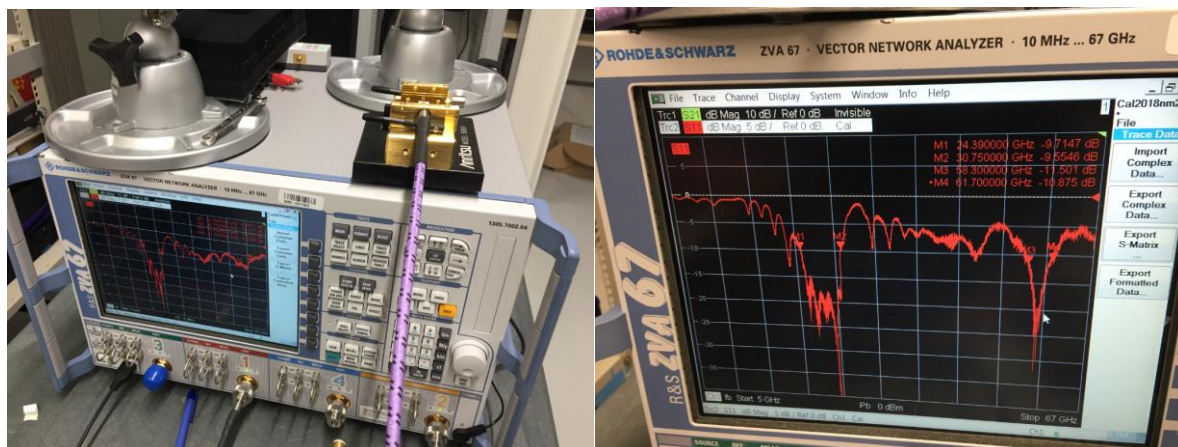
Figure 38 R&S ZVA67 vector network analyzer used for measurement

Figure 39 R&S ZVA67 vector network analyzer dynamic range [69]

5.2.3 Measurement results compared with HFSS simulations

As shown in Figure 40, the measurement data were plotted and compared with the HFSS simulation result. We can note a relatively acceptable match between the two sets of results. However, at the operating frequency, the test fixture metal impacted the radiation pattern. In fact, the large chunk of metal all around the DUT will impact the radiation tests, especially in the mm-wave bands, which has very short wavelength. Also, we used the HFSS RO3003 parameter values provided in [58], which can be another important source of discrepancies. In fact, this datasheet only provides the substrate parameter values only until 10 GHz. So, some variations can be expected between the actual performance and the datasheet declared parameters.

Furthermore, due to the lack of high-speed connectors available at the time this set of measurements was performed, we were not able to obtain the far field radiation pattern.

Figure 40 Measured and computed S_{11}

5.3 Conclusion

Three antenna arrays were fabricated on the commercial substrate of RO3003, with full ground plane at the back. The measurement results showed acceptable agreement with the HFSS simulation results.

Chapter 6. Conclusion and future work

6.1 Conclusion

This work has addressed the design of collinear circular patch antenna arrays. Fabricated on the Rogers commercial substrate RO3003, the overall antenna size is 8x25x0.5 mm^3 which is feasible to fit in mobile device chass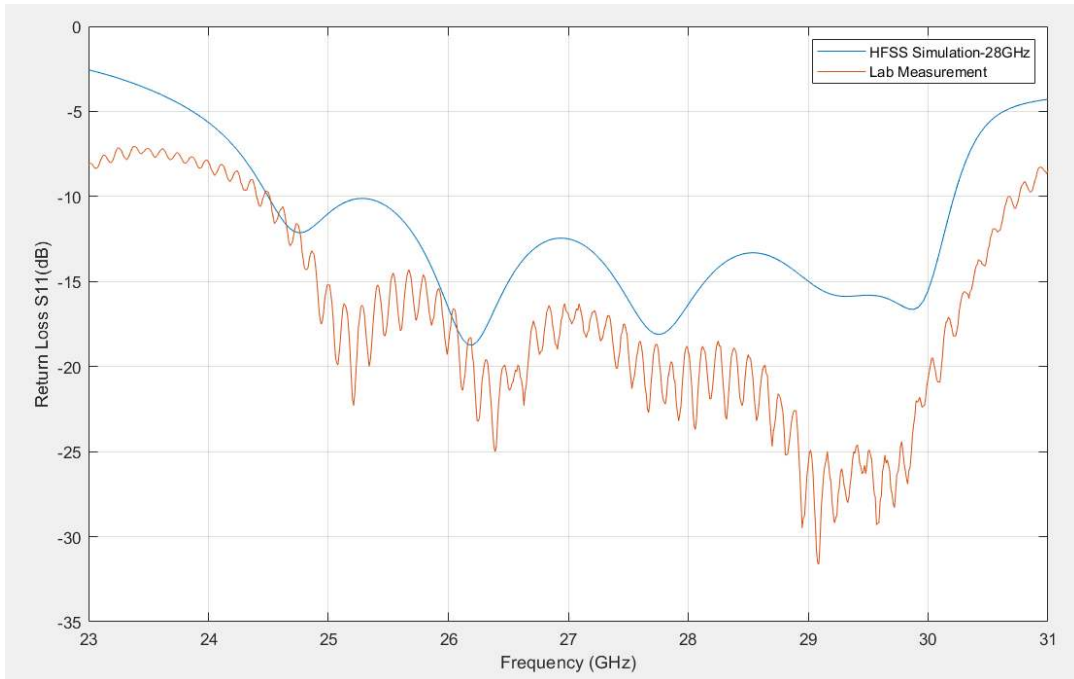is. It exhibits a measured gain over 10dBi at 28GHz and a peak gain of 10.8dB at 29GHz. The simulated radiation efficiency was 96.7%, which count for the dielectric losses while not including the mismatch losses due to later antenna connectors with users' RF board. The designed antenna is able to cover 23.6–30.3 GHz operating frequency range after optimization, which fulfill our design objective requirements.

Firstly, Critical antenna performance parameters were studied including impedance bandwidth, gain, efficiency, and radiation pattern. Also, a survey allowed to analyze different antenna types that potentially fulfill mobile device requirements regarding to size and performance.

Then, the patch antenna was selected as radiating element and a comparison between rectangular patch and circular patch showed that the circular patch performed a slightly better based on the specifically design applications and requirements. Meanwhile, substrate parameters including dielectric constant, loss tangent and thickness were investigated as well as feeding techniques. Radiation elements design models and array DDM simulation have been also included in this study.

To solve the bandwidth issue and improve gain, collinear Franklin antenna array concept was introduced and a circular array designed and fabricated, after performing an optimization round on the design parameters.

Finally, the measurement results showed relatively good match between tests and simulations, and we controlled the antenna design within a feasible size to mobile devices, with a relative high gain, wideband operating bandwidth, and high antenna efficiency.

6.2 Future Work

The first work that can be achieved in the future would be to perform the antenna far field measurements in order to demonstrate the proposed design.

Also, the proposed design performance could be further improved in terms of gain and beamforming capabilities. To do so, the following directions could be explored:

- Apply proposed antenna array on the various edges and corners of mobile devices, as presented in [18], to improve gain and coverage. However, one will need to perform a trade-off study between the device size and the feeding network design.

- Populating more subarrays, as presented in [27] and [67], using series-fed technology. This will require a trade-off consideration in these kinds of series feeding structures between enhancing the gain and widening the operating bandwidth based on the 5G evolution needs.

REFERENCES

[1]   L. J. Vora, Evolution of mobile generation technology: 1G to 5G and review of upcoming wireless technology 5G, International Journal of Modern Trends in Engineering and Research

[2]   A.C. Sountharraj, MCA. M. Phil., B. Edison, M. A. Gokul, C. N. Krishna, 5G mobile technology , American Journal of Engineering Research (AJER), Jan 2018

[3]   S. Shankland, How 5G will push a supercharged network to your phone, home, car, Mar 2nd, 2015, https://www.cnet.com/news/the-ipad-mini-is-back-but-does-it-spark-joy/

[4]   F. Boccardi et al., Commun. Mag., Five disruptive technology directions for 5G , vol. 52, no. 2, pp. 74–80, Feb. 2014.

[5]   First 5G NR specs approved, [Online]. available: http://www.3gpp.org/news-events/3gpp-news/1929-nsa nr 5g

[6]   C.-X. Wang, F. Haider, X. Gao, X.-H. You, Y. Yang, D. Yuan, H. M. Aggoune, H. Haas, S. Fletcher, and E. Hepsaydir, Cellular architecture and key technologies for 5G wireless communication networks IEEE Commun. Mag., vol. 52, no. 2, pp. 122–130, Feb. 2014.

[7]   Accessory design guidelines for Apple devices, by Apple official website download, release R7

[8]   T. A. Milligan, Modern antenna design, second edition,

[9]   S. R. Saunders and A. Aragón-Zavala, Antennas and Propagation for Wireless Communication Systems, 2nd ed. Chichester, UK: John Wiley & Sons, 2007, 554 pages.

[10]   F. C. S. Brit. Patent 242342-1924, 1924

[11]   K. SOLBACH, Microstrip-Franklin antenna , IEEE Trans. Antennas and Propagation, 1982, vol. 30, no. 4, p. 773-775.

[12]   T. F. A. Nayna ; A. K. M. Baki ; F. Ahmed, Comparative study of rectangular and circular microstrip patch antennas in X band , 2014 International Conference on Electrical Engineering and Information & Communication Technology, 2014

[13]   Characteristics of ultra-wideband technology, Rec. ITU-R SM.1755-0

[14]   C.A. Balanis, Antenna theory: analysis and design, 2nd Edition , Wiley, 2005

[15] G. R. MacCartney, J. Zhang, S. Nie, T. S. Rappaport, path loss models for 5G millimeter wave propagation channels in urban microcells. , 2013 IEEE Global Communications Conference (GLOBECOM), Exhibition & Industry Forum, 9-13.

[16] K. Klionovski, A. Shamim, M.S. Sharawi, 5G antenna array with wide-angle beam steering and dual linear polarizations, 2017 IEEE International Symposium on Antennas and Propagation & USNC/URSI National Radio Science Meeting, 2017, Page s: 1469 – 1470

[17] T. Varum, A. Ramos, J. N. Matos, Planar microstrip series-fed array for 5G applications with beamforming capabilities, 2018 IEEE MTT-S International Microwave Workshop Series on 5G Hardware and System Technologies (IMWS-5G), 2018, Page s: 1 – 3

[18] Z. U. Khan, Q. H. Abbasi, A. Belenguer, T.H. Loh, A. Alomainy, Hybrid antenna module concept for 28 GHz 5G beamsteering cellular devices, 2018 IEEE MTT-S International Microwave Workshop Series on 5G Hardware and System Technologies (IMWS-5G), 2018, Page s: 1 – 3

[19] M. S. Sharawi, M. Ikram, Slot-based connected antenna arrays for 5G mobile terminals, 2018 International Workshop on Antenna Technology (iWAT), 2018, Page s: 1 – 3

[20] X. Zhu, J.L. Zhang, T. Cui, Z.q. Zheng, A miniaturized dielectric-resonator phased antenna array with 3D-coverage for 5G mobile terminals, 2018 IEEE 5G World Forum (5GWF), 2018, Page s: 343 – 346

[21] S. F. Jilani, Q. H. Abbasi, A. Alomainy, Inkjet-printed millimetre-wave PET-based flexible antenna for 5G wireless applications, 2018 IEEE MTT-S International Microwave Workshop Series on 5G Hardware and System Technologies (IMWS-5G), 2018, Page s: 1 – 3

[22] M. Stanley, Y. Huang, H.Y. Wang, H. Zhou, A. Alieldin, S. Joseph, A novel mm-Wave phased array antenna with 360° coverage for 5G smartphone applications, 2017 10th UK-Europe-China Workshop on Millimetre Waves and Terahertz Technologies (UCMMT). 2017, Page s: 1 – 3

[23] J. Bang, Y. Hong, J. Choi, MM-wave phased array antenna for whole-metal-covered 5G mobile phone applications, 2017 International Symposium on Antennas and propagation (ISAP), 2017, Page s: 1 – 2

[24] J. Bang, J. Choi, A SAR reduced mm-Wave beam-steerable array antenna with dual-mode operation for fully metal-covered 5G cellular handsets, IEEE Antennas and Wireless Propagation Letters, 2018 , Vol. 17 , No. 6, Page s: 1118 - 1122

[25] I. Syrytsin, S. Zhang, G.F. Pedersen, A.S. Morris, Compact quad-mode planar phased array with wideband for 5G mobile terminals, IEEE Transactions on Antennas and Propagation, 2018 , Vol. 66 , No. 9, Page s: 4648 – 4657

[26] S. F. Jilani, A. Alomainy, Millimeter-wave conformal antenna array for 5G wireless applications, 2017 IEEE International Symposium on Antennas and Propagation & USNC/URSI National Radio Science Meeting, 2017, Page s: 1439 – 1440

[27] S. F. Jilani, A. Alomainy, A Multiband Millimeter-Wave 2-D Array Based on Enhanced Franklin Antenna for 5G Wireless Systems, IEEE Antennas and Wireless Propagation Letters, 2017 , Vol. 16, Page s: 2983 – 2986

[28] M. Mantash, T. A. Denidni, Millimeter-wave beam-steering antenna array for 5G applications, 2017 IEEE 28th Annual International Symposium on Personal, Indoor, and Mobile Radio Communications (PIMRC), 2017, Page s: 1 - 3

[29] H. A. Diawuo, Y.-B. Jung, Broadband proximity-coupled microstrip planar antenna array for 5G cellular applications, IEEE Antennas and Wireless Propagation Letters, 2018 , Vol. 17 , No. 7, Page s: 1286 – 1290

[30] M. Stanley, Y.Huang, T. Loh, Q. Xu, H.Y. Wang, H. Zhou, A high gain steerable millimeter-wave antenna array for 5G smartphone applications, 2017 11th European Conference on Antennas and Propagation (EUCAP), 2017, Page s: 1311 – 1314

[31] S. S. Zhu, H.W. Liu, Z.J. Chen, P. Wen, A compact gain-enhanced vivaldi antenna array with suppressed mutual coupling for 5G mm-Wave application, IEEE Antennas and Wireless Propagation Letters, 2018 , Vol. 17 , No. 5, Page s: 776 – 779

[32] U. Rafique, H. Khalil, S.U. Rehman, Dual-band microstrip patch antenna array for 5G mobile communications, 2017 Progress in Electromagnetics Research Symposium - Fall (PIERS - FALL), 2017, Page s: 55 – 59

[33] M. J. Ammann and Z. N. Chen, Wideband monopole antennas for multi-band wireless system, IEEE Antennas Propag. Mag., vol. 45, no. 2, pp. 146–150, Apr. 2003.

[34]   Z. N. Chen, Novel bi-arm rolled monopole for UWB applications, IEEE Trans. Antennas Propag., vol. 53, no. 2, pp. 672–677, Feb. 2005.

[35]   N. Behdad and K. Sarabandi, A compact antenna for ultrawide-band applications , IEEE Trans. Antennas Propagation., vol. 53, no. 7, pp.2185–2192, Jul. 2005.

[36]   J. Liang, C. C. Chiau, X. Chen, and C. G. Parini, Study of a printed circular disc monopole antenna for UWB systems, IEEE Trans. Antennas Propag., vol. 53, no. 11, pp. 3500–3504, Nov. 2005.

[37]   J. Qiu, Z. Du, J. Lu, and K. Gong, A planar monopole antenna design with band-notched characteristic," IEEE Trans. Antennas Propag., vol. 54, no. 1, pp. 288–292, Jan. 2006.

[38]   X.S. Yang; J. Salmi; A.F. Molisch; S.G. Qiu; S. Sangodoyin, B.Z. Wang, Trapezoidal monopole antenna and array for UWB-MIMO applications, Microwave and Millimeter Wave Technology (ICMMT), 2012 International Conference on. Vol. 1, 2012 , pp. 1- 4

[39]   J. Yang and A. Kishk, A novel low-profile compact directional ultrawideband antenna: the self-grounded bow-tie antenna, IEEE Transactions on Antennas and Propagation, vol. 60, no. 3, pp. 1214–1220,

[40]   H. Raza, A. Hussain, J. Yang, and P.-S. Kildal, Wideband compact 4- port dual polarized self-grounded bowtie antenna, IEEE Transactions on Antennas and Propagation, vol. 62, no. 9, pp. 4468–4473, 2

[41]   J. P. Doane, K. Sertel, and J. L. Volakis, A wideband, wide scanning tightly coupled dipole array with integrated balun (tcda-ib), IEEE Transactions on Antennas and Propagation, vol. 61, no. 9, pp. 4538– 4548,

[42]   P. Lindberg, E. Ojefors, Z. Barna, A. Thornell-Pers, and A. Rydberg, Dual wideband printed dipole antenna with integrated balun, IET microwaves, antennas & propagation, vol. 1, no. 3, pp. 707–711, 2007

[43]   J. Doane, K. Sertel, and J. Volakis, A wideband scanning conformal array with a compact compensating balun, in Antenna Applications Symposium,

[44]   T. Munekata ; M. Yamamoto ; T. Nojima, A wideband 16-element antenna array using leaf-shaped bowtie antenna and series-parallel feed networks, 2014 IEEE International Workshop on Electromagnetics (iWEM), 2014

[45] http://www.antenna-theory.com/antennas/wideband/log-periodic.php#tooth

[46] A. Neto, S. Bruni, G. Gerini, and M. Sabbadini, The Leaky Lens: A Broad-Band Fixed-Beam Leaky-Wave Antenna, IEEE Transactions on Antennas and Propagation, vol. 53, no. 10, pp. 3240–3246, 2005.

[47] E. G. Cristal, Analysis and exact design of cascaded commensurate transmission-line C-section all-pass networks, IEEE Trans. Microw. Theory Tech., vol. MTT-14, no. 6, pp. 285–291, Jun. 1966.

[48] S. Gupta, A. Parsa, E. Perret, R. V. Snyder, R. J. Wenzel, and C. Caloz, A Group-delay engineered noncommensurate transmission line all pass network for analog signal processing, IEEE Trans. Microw. Theory Tech., vol. 58, no. 9, pp. 2392–2407, Sep. 2010.

[49] R.L.Crane,All-passnetworksynthesis, IEEETrans.CircuitTheory, vol. 15, no. 4, pp. 474–477, Dec. 1968.

[50] K. Murase, R. Ishikawa, and K. Honjo, Group delay equalized monolithic microwave integrated circuit amplifier for ultra-wideband based on right/left-handed transmission line design approach, Inst. Elec. Tech. Microw. Ant. Propag., vol. 3, no. 6, pp. 967–973, 2009.

[51] J. Chen ; Q. Zhang , High scanning-rate periodic leak-wave antennas using complementary microstrip-slotline stubs , 2017 Sixth Asia-Pacific Conference on Antennas and Propagation (APCAP), Year 2017

[52] S. Liao, P. Chen, P. Wu, K. M. Shum and Q. Xue, Substrate-Integrated Waveguide-Based 60-GHz Resonant Slotted Waveguide Arrays With Wide Impedance Bandwidth and High Gain, IEEE Transactions on Antennas and Propagation, vol. 63, no. 7, pp. 2922-2931, July 2015.

[53] J. Pourahmadazar and T. A. Denidni, High Gain Substrate Integrated Waveguide Resonant Slot Antenna Array for mm-Wave Band Radio, 2015 IEEE International Conference on Ubiquitous Wireless Broadband (ICUWB), Montreal, QC, 2015, pp. 1-4.

[54] S. B. Yeap, Z. N. Chen and X. Qing, Gain-Enhanced 60-GHz LTCC Antenna Array With Open Air Cavities, IEEE Transactions on Antennas and Propagation, vol. 59, no. 9, pp. 3470-3473, Sept. 2011.

[55]   H. Jin, W. Che, K. S. Chin, G. Shen, W. Yang and Q. Xue, 60-GHz LTCC Differential-Fed Patch Antenna Array With High Gain by Using Soft-Surface Structures, in IEEE Transactions on Antennas and Propagation, vol. 65, no. 1, pp. 206-216, Jan. 2017.

[56]   S. Liao and Q. Xue, Dual Polarized Planar Aperture Antenna on LTCC for 60-GHz Antenna-in-Package Applications, in IEEE Transactions on Antennas and Propagation, vol. 65, no. 1, pp. 63-70, Jan. 2017.

[57]   D. Psychoudakis, A. Foroozesh, Small millimeter wave printed antenna arrays for 5G applications, 2017 IEEE International Symposium on Antennas and Propagation & USNC/URSI National Radio Science Meeting, 2017, Page s: 1805 – 1806

[58]   Rogers RO3000 Laminate datasheet, https://www.rogerscorp.com/documents/722/acs/RO3000-Laminate-Data-Sheet-RO3003-RO3006-RO3010.pdf

[59]   I. F. da Costa, S. Arismar Cerqueira, D. H. Spadoti, Dual-band slotted waveguide antenna array for adaptive mm-wave 5G networks, 2017 11th European Conference on Antennas and Propagation (EUCAP), 2017, Page s: 1322 – 1325

[60]   B. J. Kwaha, 1O. N Inyang and P. Amalu, The Circular Microstrip Patch Antenna- Design and Implementation, IJRRAS, Vol 8, Issue 1, 2011

[61]   W. L. Stutzman, G. A. T. Hoboken , Antenna theory and design, 3rd ed , NJ, USA: John Wiley & Sons, 2011, 822 pages.

[62]   A. C. Tengli , P. M. Hadalgi, Design of inset-fed penta-band circular microstrip antenna for wireless and X-band communication , International Journal of Advanced Research in Electrical, Electronics and Instrumentation Engineering (An UGC Approved Journal) , Vol. 6, Issue 8, August 2017

[63]   J. R. Panda, R. S. Kshetrimayum, An inset-fed dual-frequency circular microstrip antenna with a rectangular slot for application in wireless communication,

[64]   G.A. E. Vandenbosch, A. Vasylchenko, A Practical Guide to 3D Electromagnetic Software Tools, Katholieke Universiteit Leuven Belgium

[65]   Z. N. Chen, M. Y. W. Chia, Broadband planar antennas: Design and applications, 1st Edition. , Chichester, UK: John Wiley & Sons, 2006, p. 243.

[66]   HFSS Antenna Design Kit emended in Ansoft HFSS software v19.2

[67] T. Varum, A. Ramos, J. N. Matos, Planar microstrip series-fed array for 5G applications with beamforming capabilities, 2018 IEEE MTT-S International Microwave Workshop Series on 5G Hardware and System Technologies (IMWS-5G), 2018, Pages: 1 – 3

[68] 3680 Series Universal Test Fixture Operation and Maintenance Manual, published on Anritsu official website

[69] R&S®ZVA Vector Network Analyzer Specifications, published on Rohde & Schwarz office website

[70] A. Alipour,, H.R. Hassani , A novel omni-directional UWB monopole antenna, Antennas and Propagation, IEEE Transactions on , Vol. 56, No. 12, 2012 , pp. 2837- 2840

[71] A. Najam, Y. Duroc, and S. Tedjni, UWB-MIMO Antenna with novel stub structure, Progress In Electromagnetics Research C, Vol. 19, pp. 245-257, 2011

[72] A. Bekasiewicz; S. Koziel, A concept and design optimization of compact planar UWB monopole antenna, Antennas and Propagation Society International Symposium (APSURSI), 2014 IEEE,2014 , pp. 1813- 1814

[73] G.K. Pandey; H.S. Singh; P.K. Bharti; M.K. Meshram, UWB monopole antenna with enhanced gain and stable radiation pattern using gate like structures, Microwave and Photonics (ICMAP), 2013 International Conference on, 2013 , pp. 1- 4

[74] N. P. Agarwall; G. Kumar; K. P. Ray; Wide-band planar monopole antennas, IEEE Trans. Antennas Propagation, Vol. 46, No. 2, 1998, pp. 294-295.

[75] R. Singh, Broadband planar monopole antennas, M.Tech credit seminar report, Electronic Systems group, EE Dept, IIT Bombay submitted Nov 03.

[76] N. P. Agarwall; G. Kumar; K. P. Ray; Wide-band planar monopole antennas, IEEE Trans. Antennas Propagation, Vol. 46, No. 2, 1998, pp. 294-295.

[77] M. J. Ammann; Z.N. Chen; An asymmetrical feed arrangement for improved impedance bandwidth of planar monopole microwave and optical technology, Vol. 40, No. 2.; January 20 2004.